Copy 341

NASA TM X-49

NASA TM X-40

c. 341

LOAN COPY: RETURN TO
AFWL (WLL—)
KIRTLAND AFB, N MEX

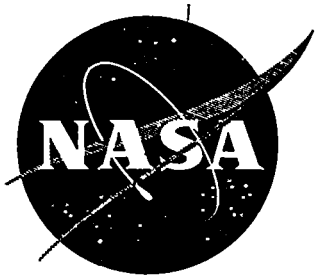

TECHNICAL MEMORANDUM

X - 40

TRANSONIC STATIC AERODYNAMIC CHARACTERISTICS OF A BLUNT CONE-CYLINDER BODY WITH FLARED AFTERBODY OR BLUNT CRUCIFORM FINS

By Earl D. Knechtel, Stuart L. Treon,
and Roy M. Wakefield

Ames Research Center
Moffett Field, Calif.

CLASSIFIED DOCUMENT - TITLE UNCLASSIFIED

This material contains information affecting the national defense of the United States within the meaning of the espionage laws, Title 18, U.S.C., Secs. 793 and 794, the transmission or revelation of which in any manner to an unauthorized person is prohibited by law.

NATIONAL AERONAUTICS AND SPACE ADMINISTRATION

WASHINGTON August 1959

SWC 9 C549 72/341

```
--     1   OF     1
-- 1 -  AD NUMBER: 309765
-- 2 -  FIELDS AND GROUPS: 20/4
-- 3 -  ENTRY CLASSIFICATION:    UNCLASSIFIED
-- 5 -  CORPORATE AUTHOR: NATIONAL AERONAUTICS AND SPACE ADMINISTRATION
--      WASHINGTON D C
-- 6 -  UNCLASSIFIED TITLE:      TRANSONIC STATIC AERODYNAMIC
--      CHARACTERISTICS OF A BLUNT CONE-CYLINDER BODY WITH FLARED AFTERBODY
--      OR BLUNT CRUCIFORM FINS
-- 8 -  TITLE CLASSIFICATION:    UNCLASSIFIED
-- 9 -  DESCRIPTIVE NOTE: TECHNICAL MEMO.,
--10 -  PERSONAL AUTHORS: KNECHTEL,EARL D.;TREON,STUART L.;WAKEFIELD,ROY M.;
--11 -  REPORT DATE:       AUG    , 1959
--12 -  PAGINATION:      49P    MEDIA COST:   $   6.00
--14 -  REPORT NUMBER:     NASA-TM-X-40
--20 -  REPORT CLASSIFICATION:  UNCLASSIFIED
--21 -  SUPPLEMENTARY NOTE:      ALSO AVAILABLE FROM NASA AS TECHNICAL MEMO.
--      NO. X-40.
--23 -  DESCRIPTORS:       *BLUNT BODIES, *TRANSONIC CHARACTERISTICS, BODIES
--      OF REVOLUTION, CYLINDRICAL BODIES, STABILITY
--24 -  DESCRIPTOR CLASSIFICATION:    UNCLASSIFIED
--33 -  LIMITATION CODES:  2
--35 -  SOURCE CODE:       240400
-
--36 -  ITEM LOCATION:      DTIC
--40 -  GEOPOLITICAL CODE:       1100
--41 -  TYPE CODE:  Z
--43 -  IAC DOCUMENT TYPE:
```

TECH LIBRARY KAFB, NM
0093933

2 cds removed 18 Dec 63 fa

[redacted]

NATIONAL AERONAUTICS AND SPACE ADMINISTRATION

TECHNICAL MEMORANDUM X-40

TRANSONIC STATIC AERODYNAMIC CHARACTERISTICS OF A BLUNT CONE-CYLINDER BODY WITH FLARED AFTERBODY OR BLUNT CRUCIFORM FINS*

By Earl D. Knechtel, Stuart L. Treon,
and Roy M. Wakefield

SUMMARY

An experimental investigation has been conducted in a transonic wind tunnel to determine the static aerodynamic characteristics of a low-fineness-ratio blunt cone-cylinder stabilized either by a flared afterbody or by blunt cruciform fins of the same plan form. For two plan forms (flare angles of 20° and 30°), the relative effectiveness of fins and flare is shown in terms of normal force, forebody and base axial forces, and pitching moment. For the finned models, the effects of roll angle on these components as well as on rolling moment are presented. Test Mach numbers ranged from 0.6 to 1.4 and angles of attack from -2° to $+14^{\circ}$, for a constant Reynolds number of 0.375 million based upon the cylindrical body diameter.

INTRODUCTION

Recent increased demand for aerodynamic data on low-fineness-ratio bodies of revolution at transonic speeds stems not only from the growing interest in atmosphere entry vehicles and aircraft escape capsules, but also from an increasing awareness that stability of such bodies is often critical in the transonic speed range. Experimental studies of low-fineness-ratio blunt bodies at transonic speeds, such as that of reference 1, are not sufficiently numerous to provide data over the ranges of design parameters of interest.

As part of an experimental study of the transonic aerodynamic characteristics of a number of low-fineness-ratio blunt bodies, the present report shows results for a blunt cone-cylinder with flared afterbodies and cruciform fins having the same plan form. The results are published without detailed discussion.

---

*Title, Unclassified

[redacted]

1341

[redacted]

NOTATION

C_{A_f}	forebody axial-force coefficient, $\frac{\text{forebody axial force}}{qS}$
C_{A_b}	base axial-force coefficient, $\frac{\text{base axial force}}{qS}$
C_l	rolling-moment coefficient, $\frac{\text{rolling moment}}{qSd}$
C_m	pitching-moment coefficient about nose-body juncture, $\frac{\text{pitching moment}}{qSd}$
C_N	normal-force coefficient, $\frac{\text{normal force}}{qS}$
c.p.	center-of-pressure location
d	cylindrical body diameter
M	Mach number
q	dynamic pressure
S	cross-sectional area of cylindrical body
α	angle of attack, deg
φ	angle of roll, deg (see fig. 1(c))

Model Component Designations

N_2	blunt conical nose
$B_2, B_{2.9}, B_{3.4}$	cylindrical body, subscript indicating length in body diameters
F_{20-4}, F_{30-4}	flared afterbody, subscripts indicating flare angle and ratio of base area to body cross-sectional area
C_{20}, C_{30}	blunt cruciform fins, subscript indicating leading-edge semivertex angle in degrees

[redacted]

APPARATUS AND MODELS

The investigation was conducted in the Ames 2- by 2-foot transonic wind tunnel, which is of the closed-circuit, variable-pressure type. This facility has a flexible nozzle followed by a porous test section which permits continuous choke-free operation at Mach numbers up to 1.4. Additional details regarding this facility are presented in reference 2.

Dimensioned sketches of the six models employed in this investigation are shown in figure 1. A blunt conical nose and cylindrical center body 2 diameters long were common to all of the models. This basic shape was tested in turn with a flared afterbody, a cylindrical afterbody having blunt cruciform fins of the same plan form as the flared afterbody, and a simple cylindrical afterbody of equal length. Fin and flare angles of 20° and 30° were investigated for a flare length sufficient in each case to make the base diameter twice that of the cylindrical body. A boundary-layer trip wire of 0.008-inch diameter was cemented around the conical surface 1/2 inch behind the tip of the nose.

The models were mounted in the test section on a sting-supported internal strain-gage balance. Photographs of two of the models in the test section are shown in figure 2.

TESTS, DATA REDUCTION, AND PRECISION

The investigation was conducted at ten Mach numbers from 0.6 to 1.4, eleven angles of attack from -2° to $+14^\circ$, and a constant Reynolds number of 0.375 million based on the cylindrical body diameter. Normal force, axial force, and pitching moment were measured for all models. In addition, rolling moment was measured for the finned models, which were tested at roll angles of 0°, $22\text{-}1/2^\circ$, and 45° with respect to the pitch plane and balance.

Preliminary studies employing the boundary-layer visualization technique of reference 3 indicated that the boundary-layer flow over the blunt conical nose naturally became turbulent on the forepart of the conical surface; hence the boundary layer would also be expected to be turbulent at the higher Reynolds numbers of full-scale flight conditions. To ensure uniformly turbulent boundary-layer conditions, an 0.008-inch-diameter trip wire was employed on the conical nose surface.

The forebody axial-force coefficients were obtained by adjusting the measured axial forces to correspond to a condition of free-stream static pressure over the entire base area of each model. The effects of sting interference on base drag are known (ref. 4) to be significant for cylindrical bodies at and above sonic speed and, although not known for

the present finned and flared models, are presumed to vary with such changes in model geometry. For possible reference, values of base axial-force coefficient were also obtained.

The angles of attack have been corrected for elastic deflection of the balance and sting under aerodynamic loads. Stream-angularity corrections in this wind tunnel are known to be negligible and therefore were not applied.

No corrections have been made for possible interference effects of the porous test-section walls. However, in the appendix to reference 5, an approximate analytical expression was given for the Mach number shift at sonic speed caused by interference between a porous test section and a small model. Application of this formula to the present configurations indicates that wall interference would cause true sonic speed to occur at a test Mach number of approximately 1.05. However, transonic tests of various sizes of sharp- and blunt-nosed bodies reported in the appendix to reference 6 indicated no significant systematic effects of wall interference for models approximately the size of those of the present test. Therefore it is believed that there is no serious error in neglecting wall-interference effects in the present results.

In addition to the possible systematic errors resulting from neglecting some of the above corrections, certain random errors exist which influence the precision, or repeatability, of the results. An analysis using the methods of reference 7 indicated that the precision of Mach number, angle of attack, and aerodynamic coefficients was as follows:

M	0.003
α	0.05°
C_N	0.02
C_m	0.03
C_{A_f}	0.02
C_{A_b}	0.01
C_l	0.03

RESULTS

The basic variations with angle of attack of coefficients of normal force, pitching moment, forebody axial force, and base axial force for configurations having cylindrical, flared, and finned afterbodies are presented in figures 3 to 10, and the effects of roll angle on the longitudinal and rolling characteristics of the finned configurations are shown in figures 11 through 18. The variations with Mach number of normal-force parameter C_N/α and center of pressure at three angles of attack, and of forebody and base axial-force coefficients at zero angle of attack are summarized in figures 19, 20, 21, and 22, respectively. In figure 23, shadowgraph views of the two flared models near 0° angle of attack are presented to show the difference in flow pattern before and after the onset of flow separation ahead of the flares. The separation was observed to have a significant effect on the longitudinal characteristics of these models, particularly on the normal-force parameter and center of pressure. No such flow separation was observed for the models with the cylindrical or finned afterbodies.

Ames Research Center
National Aeronautics and Space Administration
Moffett Field, Calif., April 14, 1959

[redacted]

REFERENCES

1. Fisher, Lewis R., Keith, Arvid L., Jr., and DiCamillo, Joseph R.: Aerodynamic Characteristics of Some Families of Blunt Bodies at Transonic Speeds. NASA MEMO 10-28-58L, 1958.

2. Spiegel, Joseph M., and Lawrence, Leslie F.: A Description of the Ames 2- by 2-Foot Transonic Wind Tunnel and Preliminary Evaluation of Wall Interference. NACA RM A55I21, 1956.

3. Main-Smith, J. D.: Chemical Solids as Diffusible Coating Films for Visual Indications of Boundary-Layer Transition in Air and Water. R. & M. No. 2755, British, 1950.

4. Lee, George, and Summers, James L.: Effects of Sting-Support Interference on the Drag of an Ogive-Cylinder Body With and Without a Boattail at 0.6 to 1.4 Mach Number. NACA RM A57I09, 1957.

5. Page, William A.: Experimental Study of the Equivalence of Transonic Flow About Slender Cone-Cylinders of Circular and Elliptic Cross Section. NACA TN 4233, 1958.

6. Treon, Stuart L.: The Effect of Nose Shape on the Static Aerodynamic Characteristics of Ballistic-Type Missile Models at Mach Numbers from 0.6 to 1.4. NASA MEMO 5-17-59A, 1959.

7. Beers, Yardley: Introduction to the Theory of Error. Addison-Wesley Publishing Co., Cambridge, Mass., 1953.

[redacted]

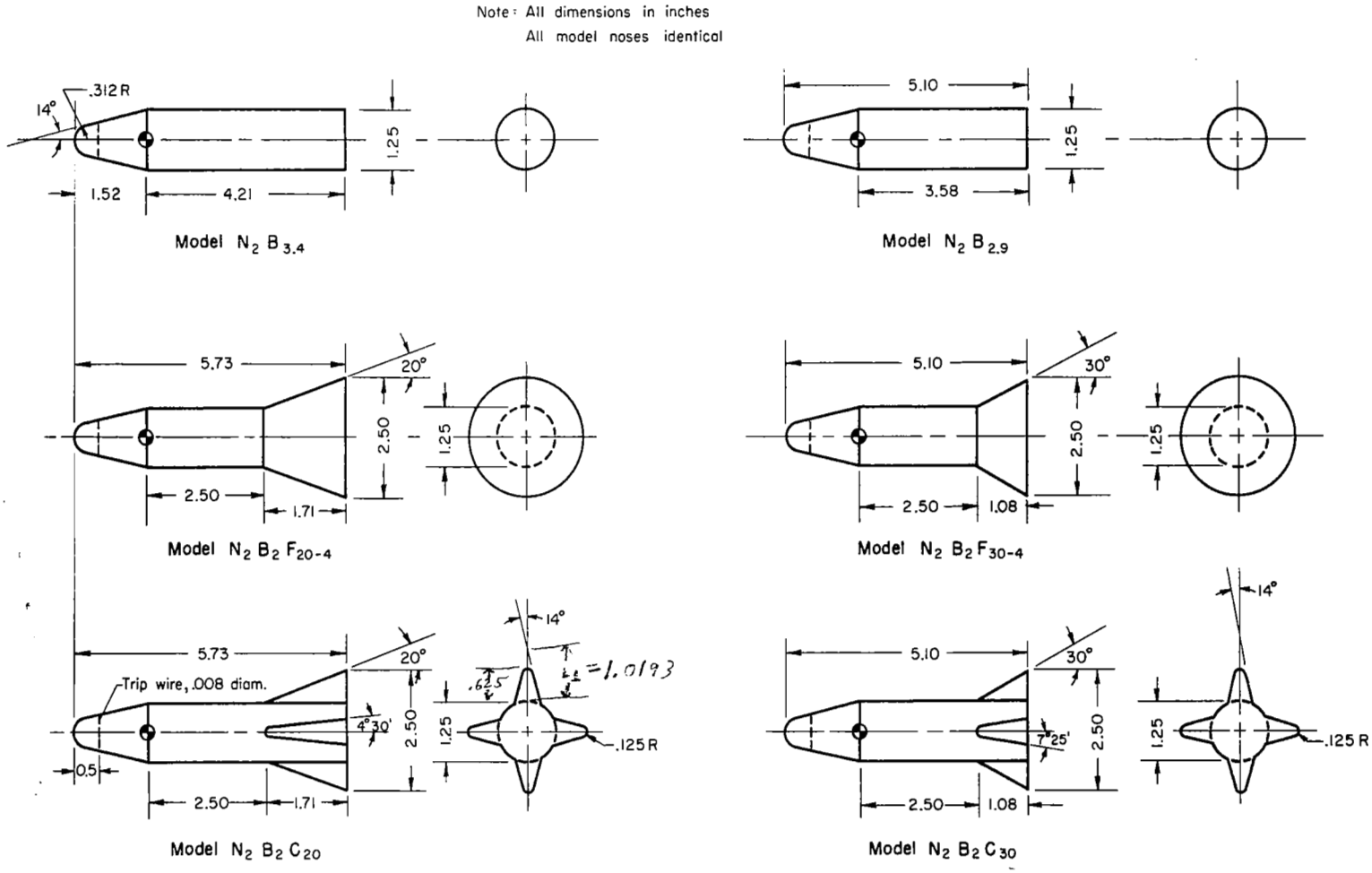

(a) Models

Figure 1.- Geometric details of models and shroud.

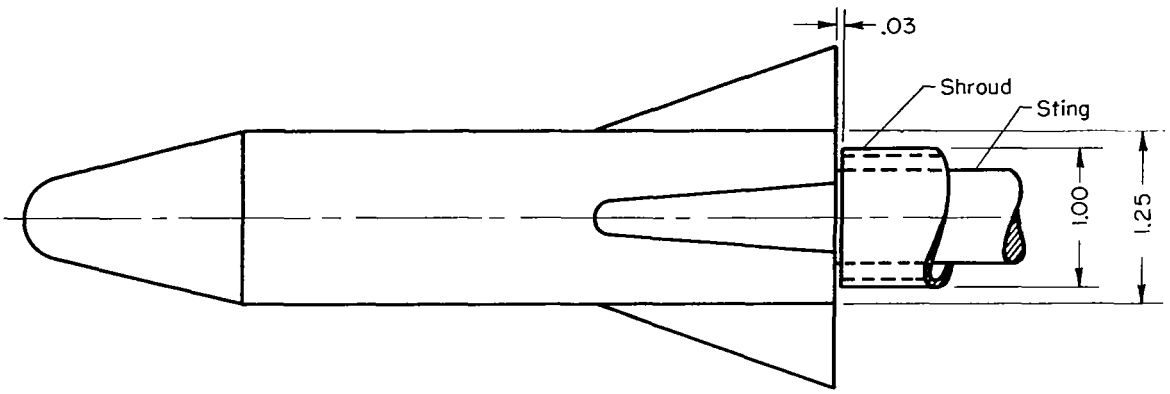

(b) Shroud arrangement for typical model.

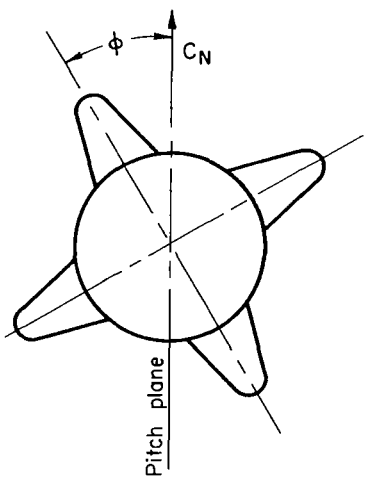

Front view

(c) Roll-angle definition for finned model.

Figure 1.- Concluded.

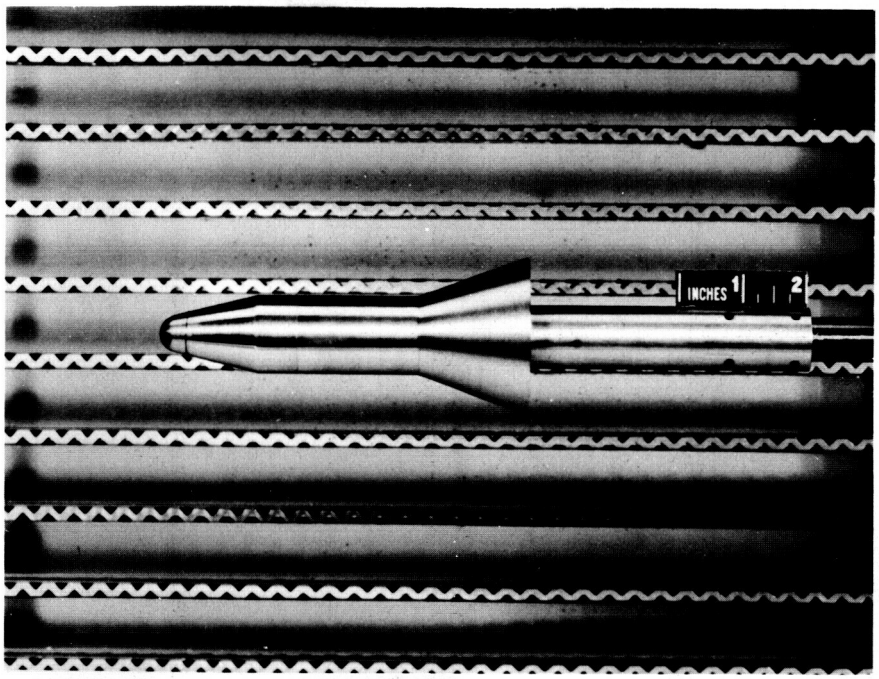

A-24665

(a) $N_2B_2F_{20-4}$

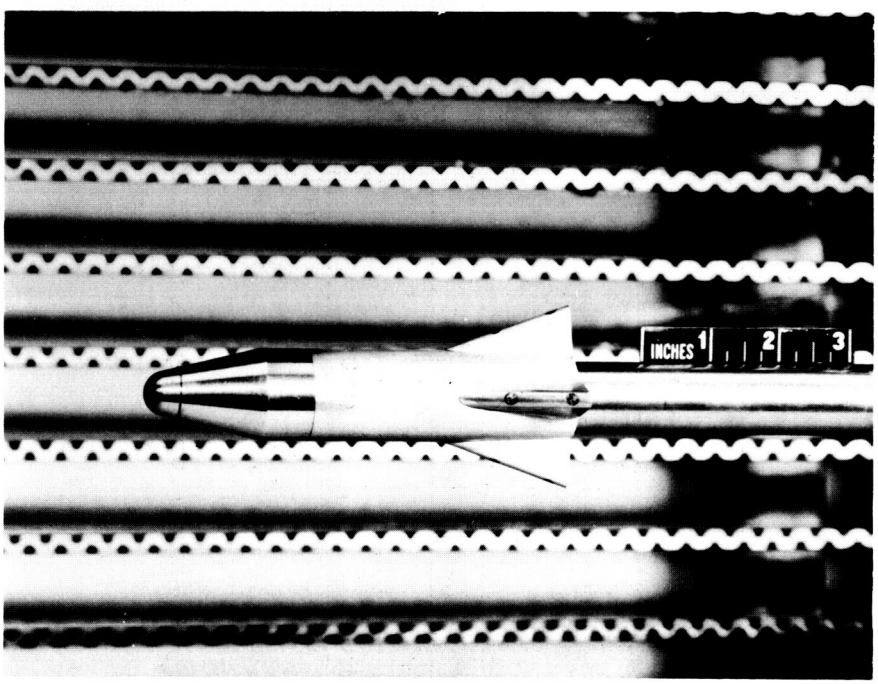

A-24676

(b) $N_2B_2C_{20}$

Figure 2.- Typical models mounted in the Ames 2- by 2-foot transonic wind tunnel.

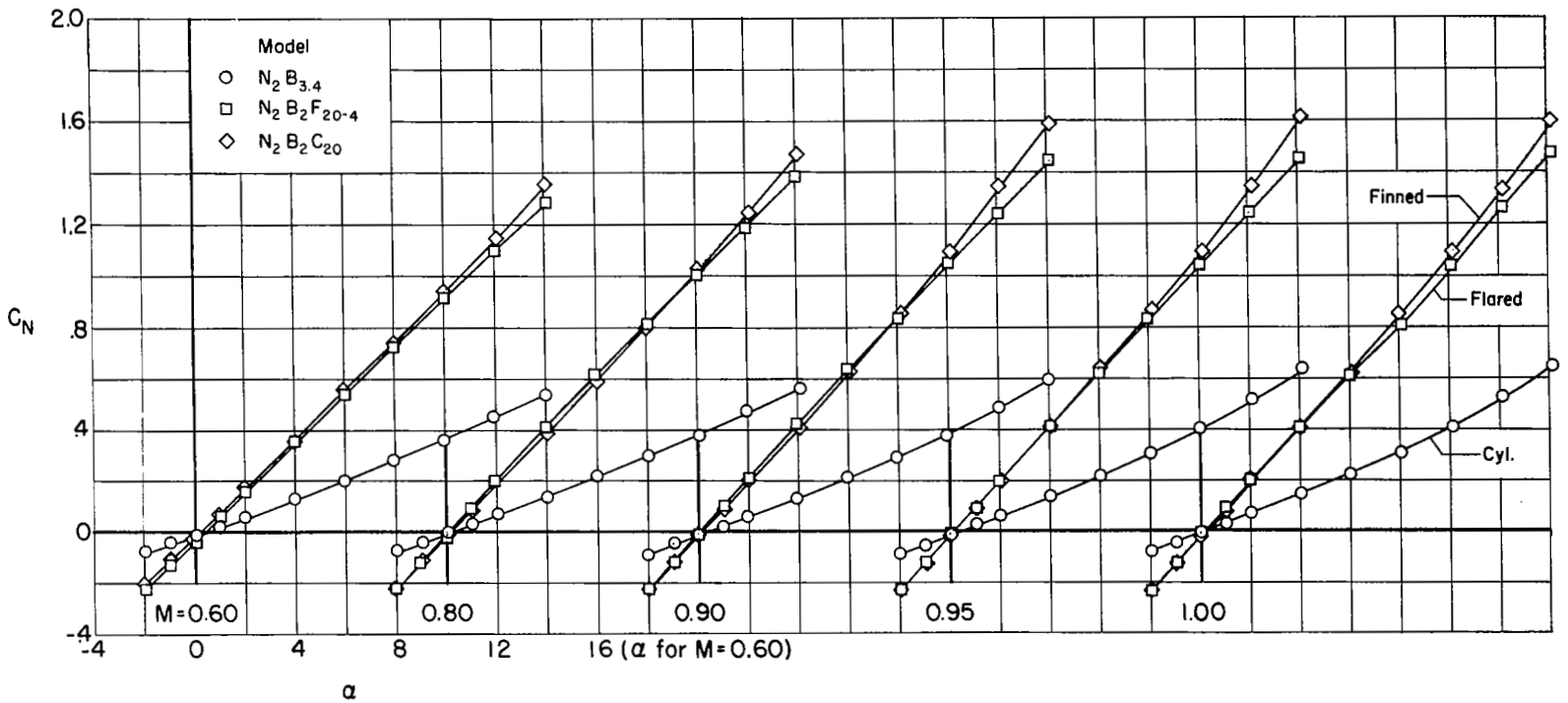

(a) M = 0.60 to 1.00

Figure 3.- Normal-force coefficients for models having flared or finned afterbody plan forms of 20° semivertex angle, or cylindrical afterbody.

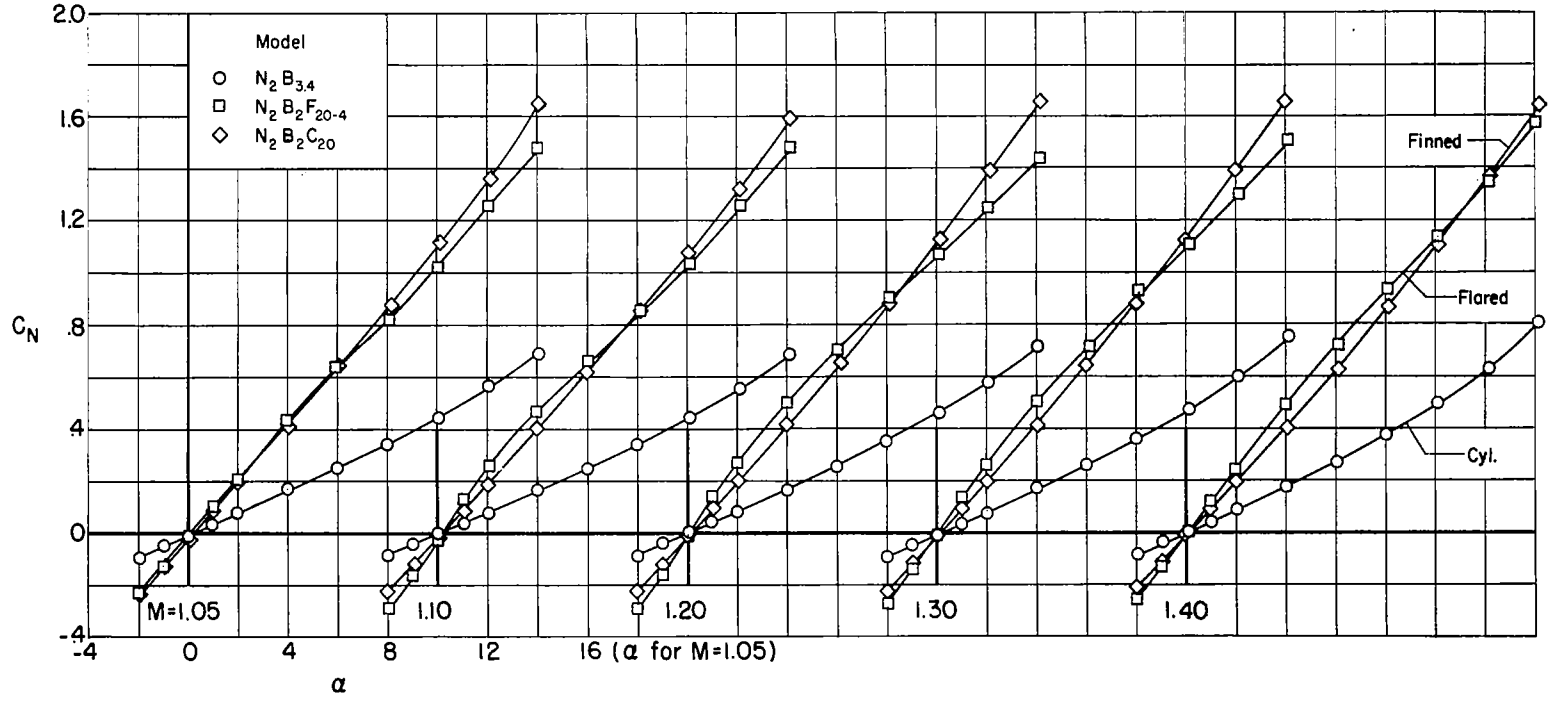

(b) M = 1.05 to 1.40

Figure 3.- Concluded.

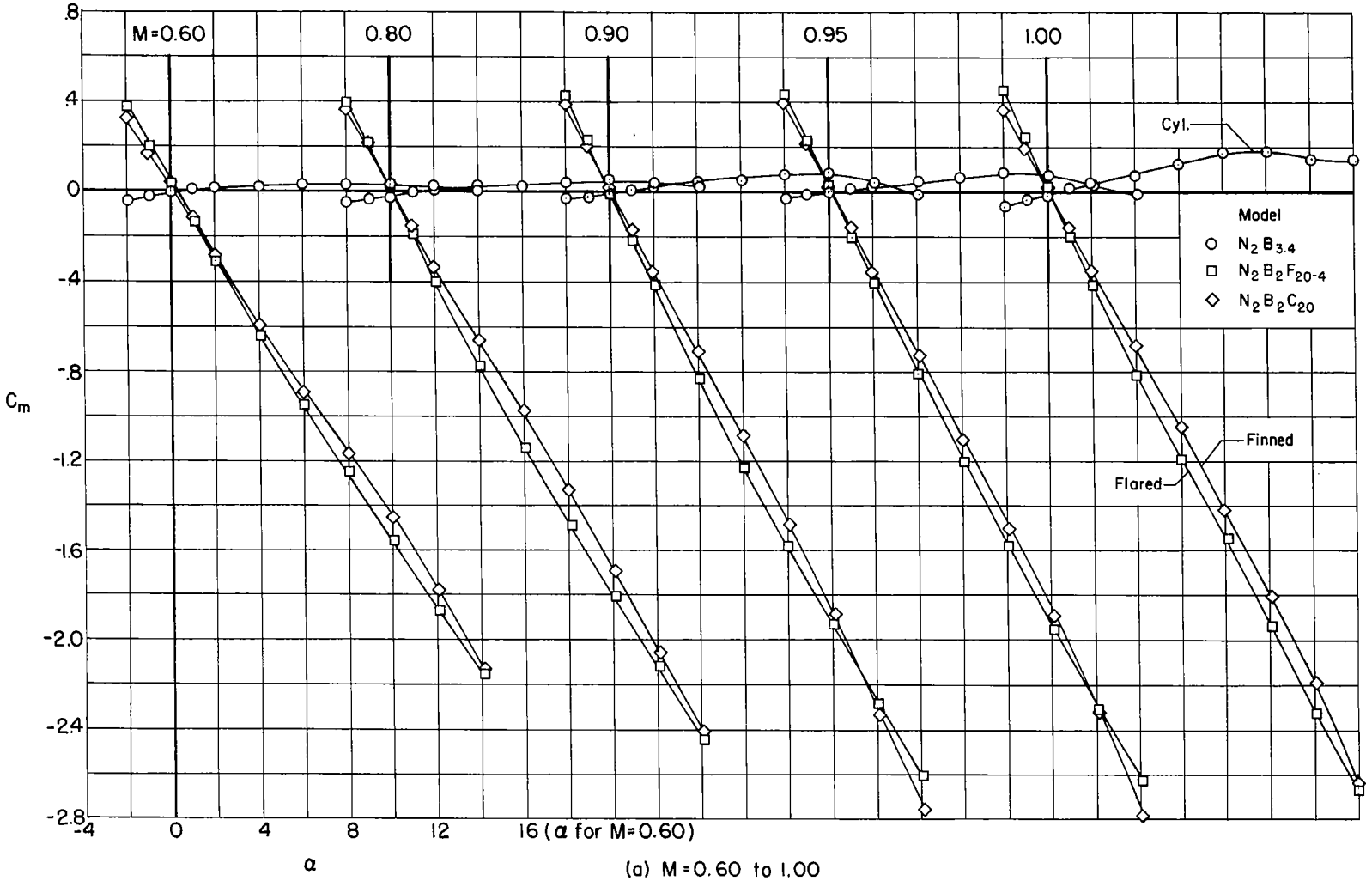

(a) M = 0.60 to 1.00

Figure 4.- Pitching-moment coefficients for models having flared or finned afterbody plan forms of 20° semivertex angle, or cylindrical afterbody.

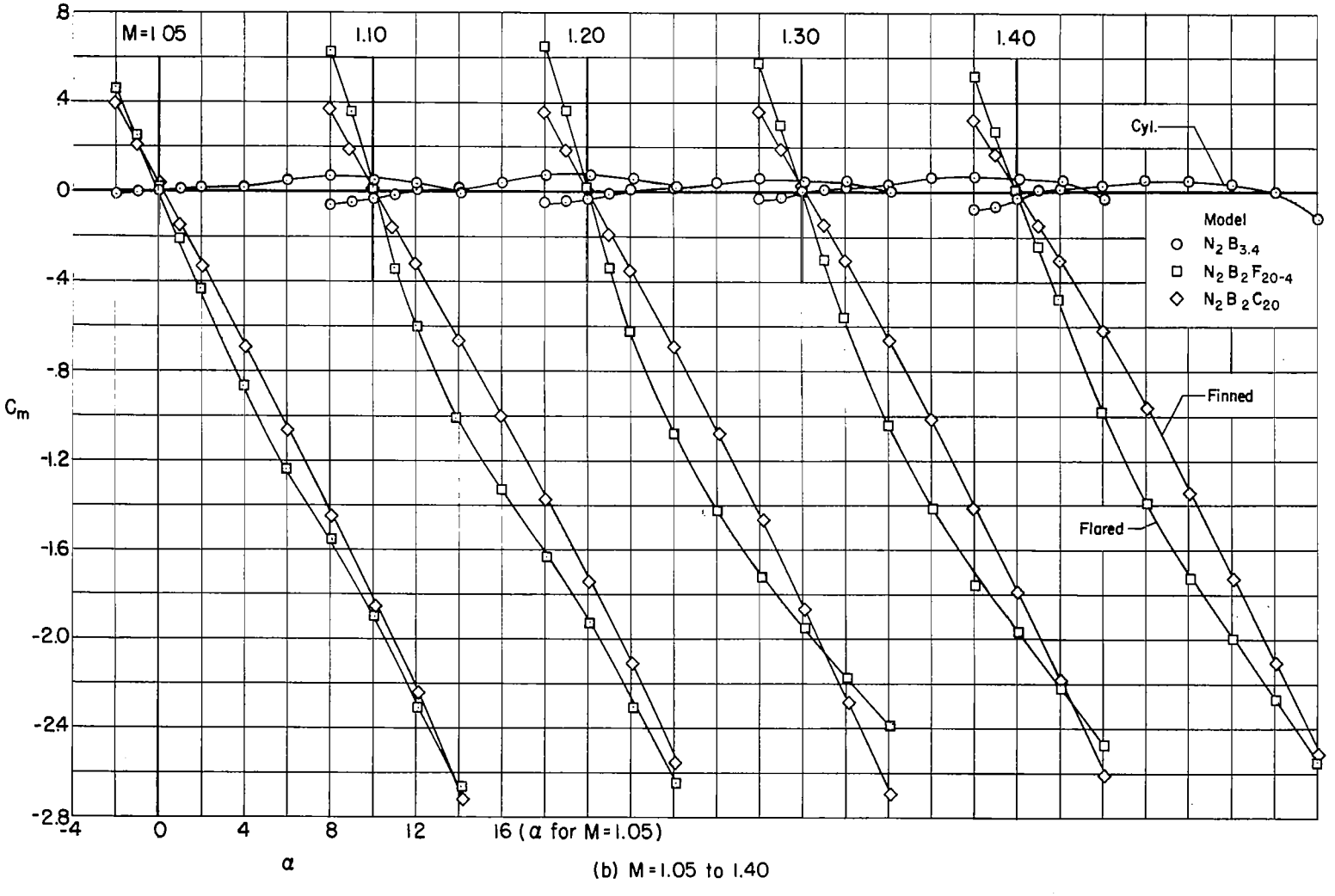

(b) M=1.05 to 1.40

Figure 4.- Concluded.

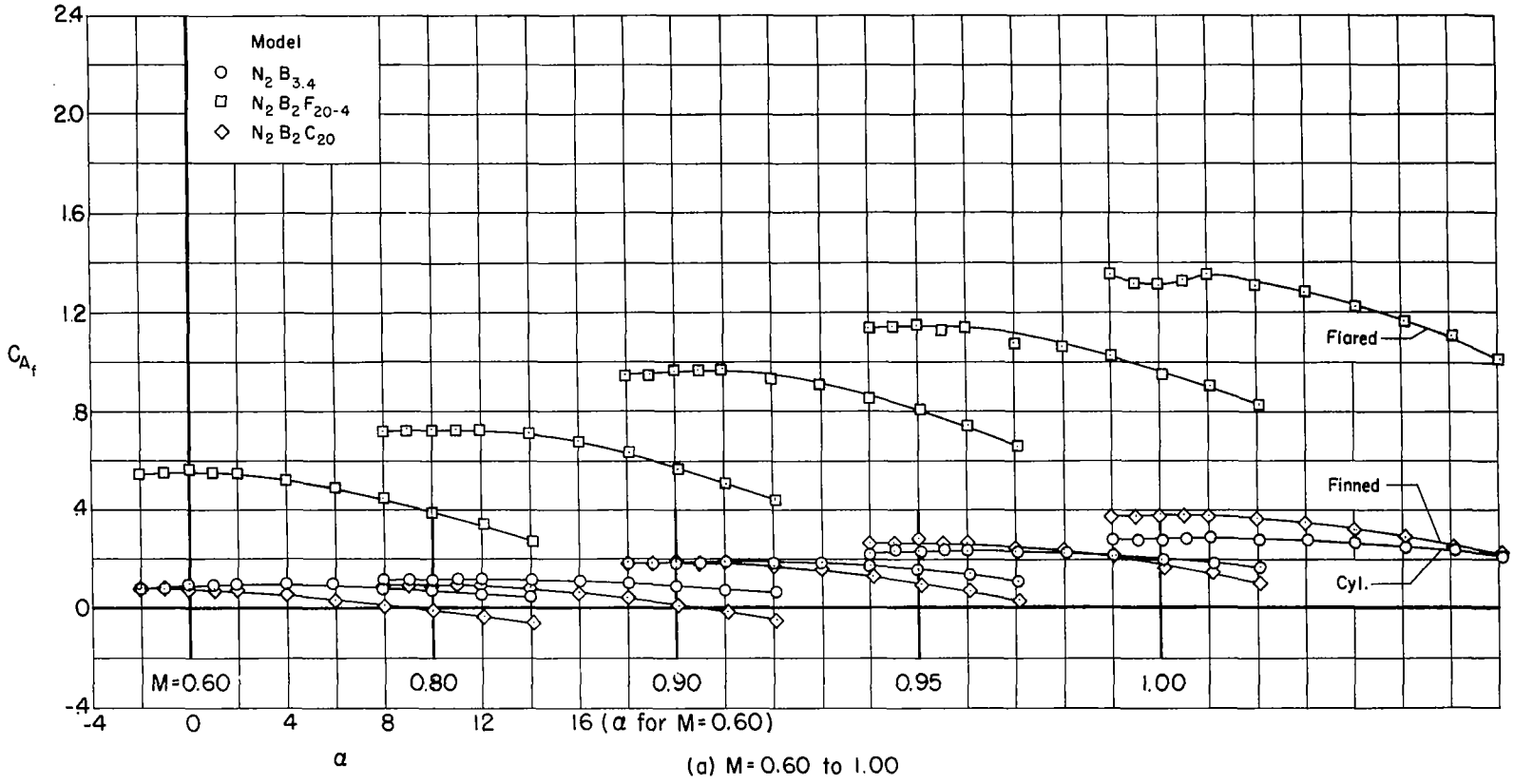

(a) M = 0.60 to 1.00

Figure 5.- Forebody axial-force coefficients for models having flared or finned afterbody plan forms of 20° semivertex angle, or cylindrical afterbody.

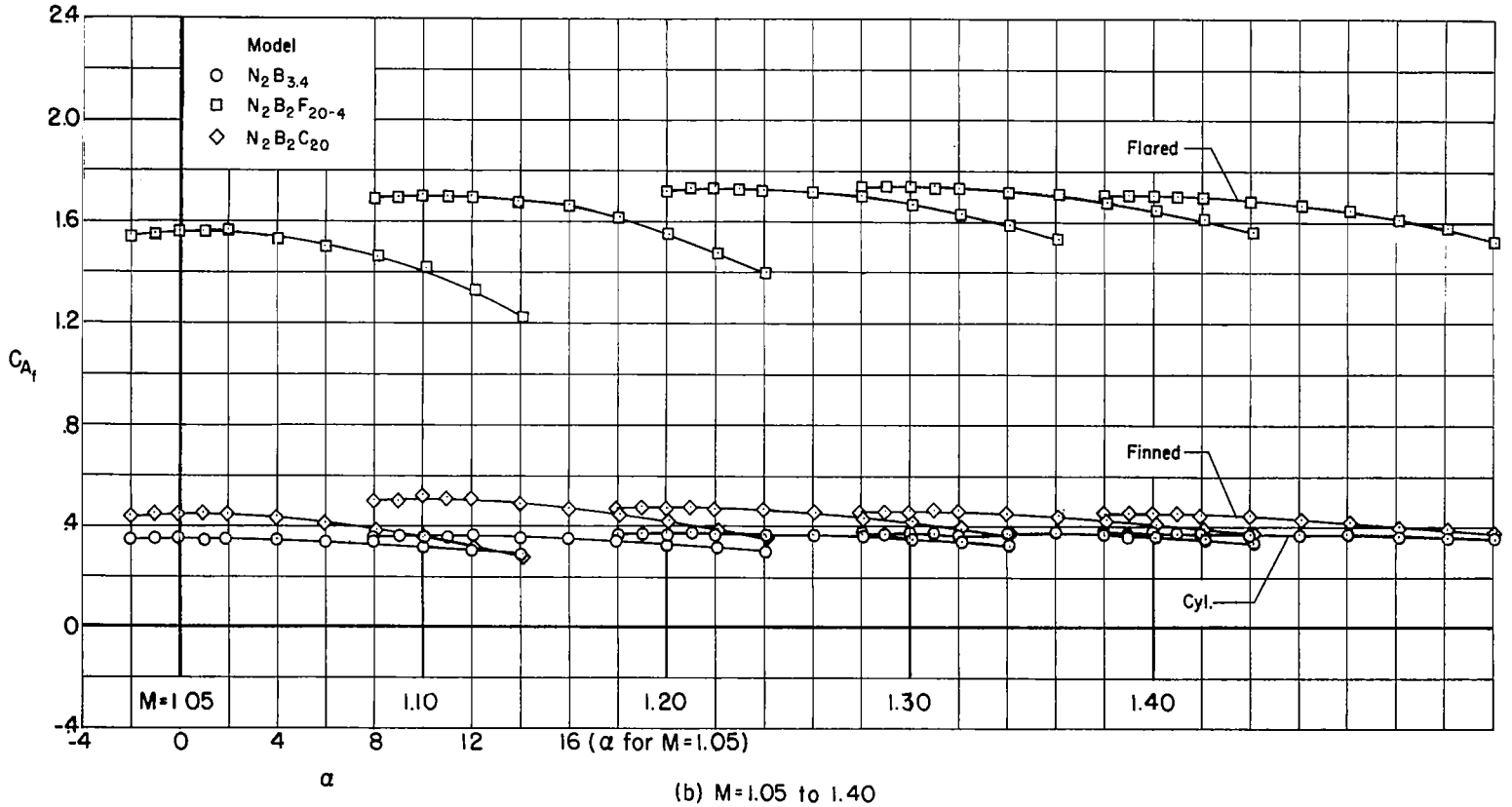

(b) M=1.05 to 1.40

Figure 5.- Concluded.

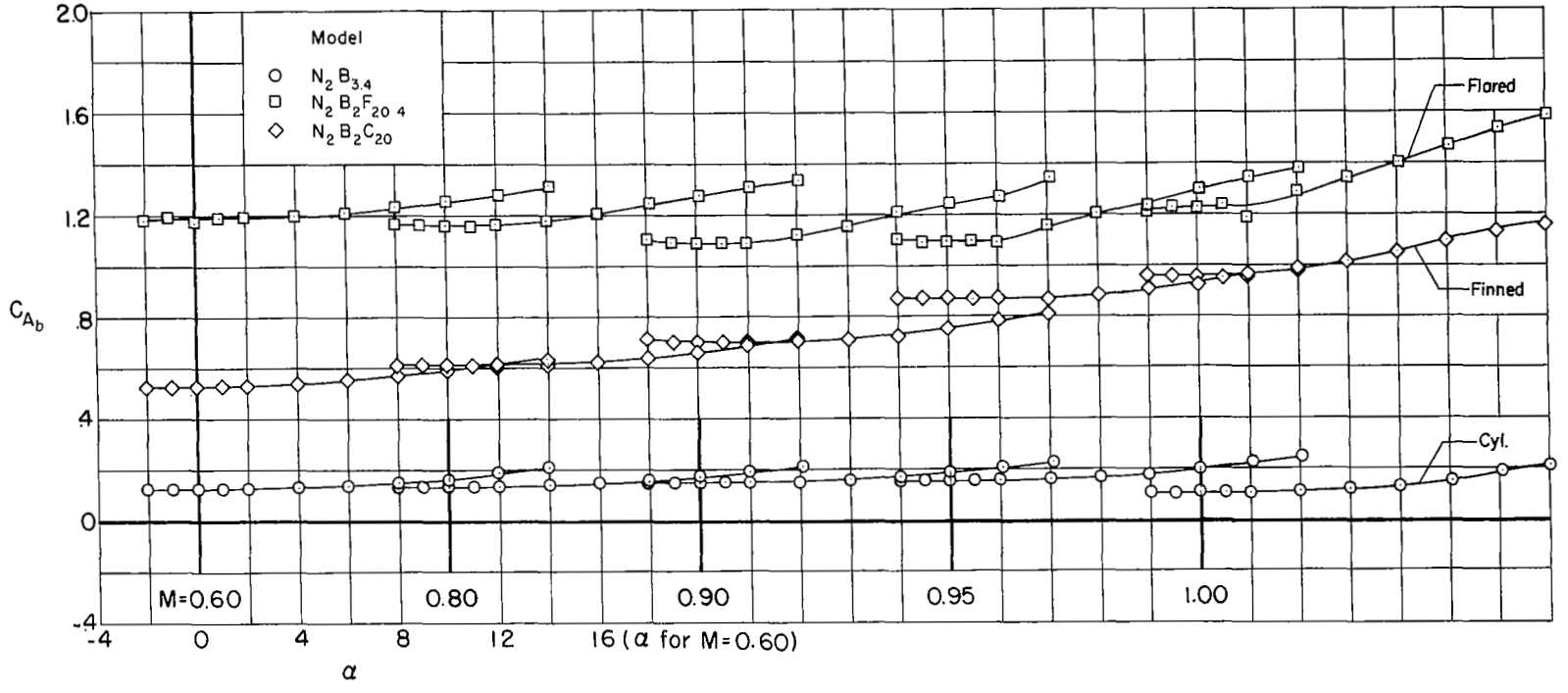

(a) M = 0.60 to 1.00

Figure 6.- Base axial-force coefficients for models having flared or finned afterbody plan forms of 20° semivertex angle, or cylindrical afterbody.

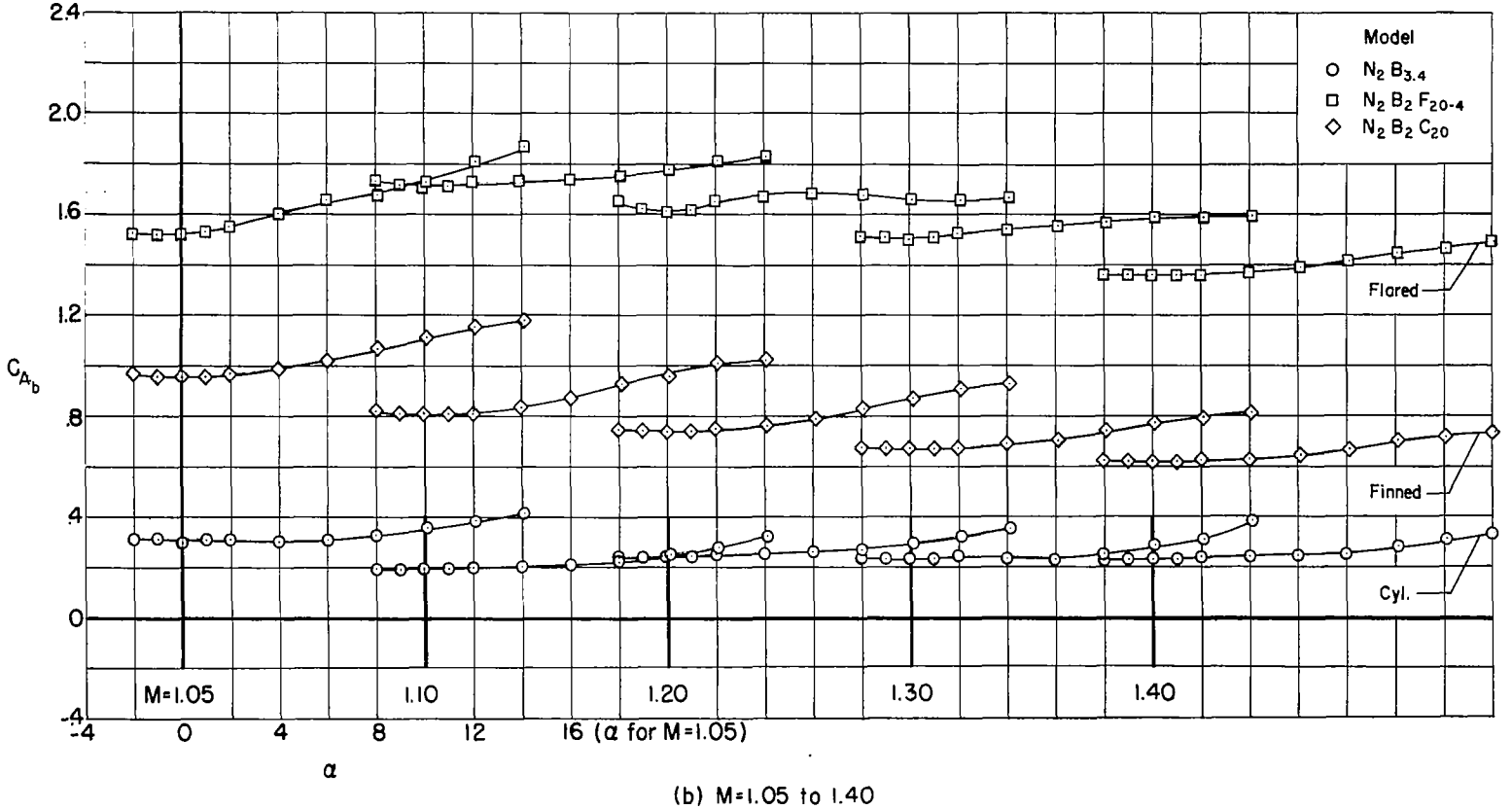

(b) M=1.05 to 1.40

Figure 6.- Concluded.

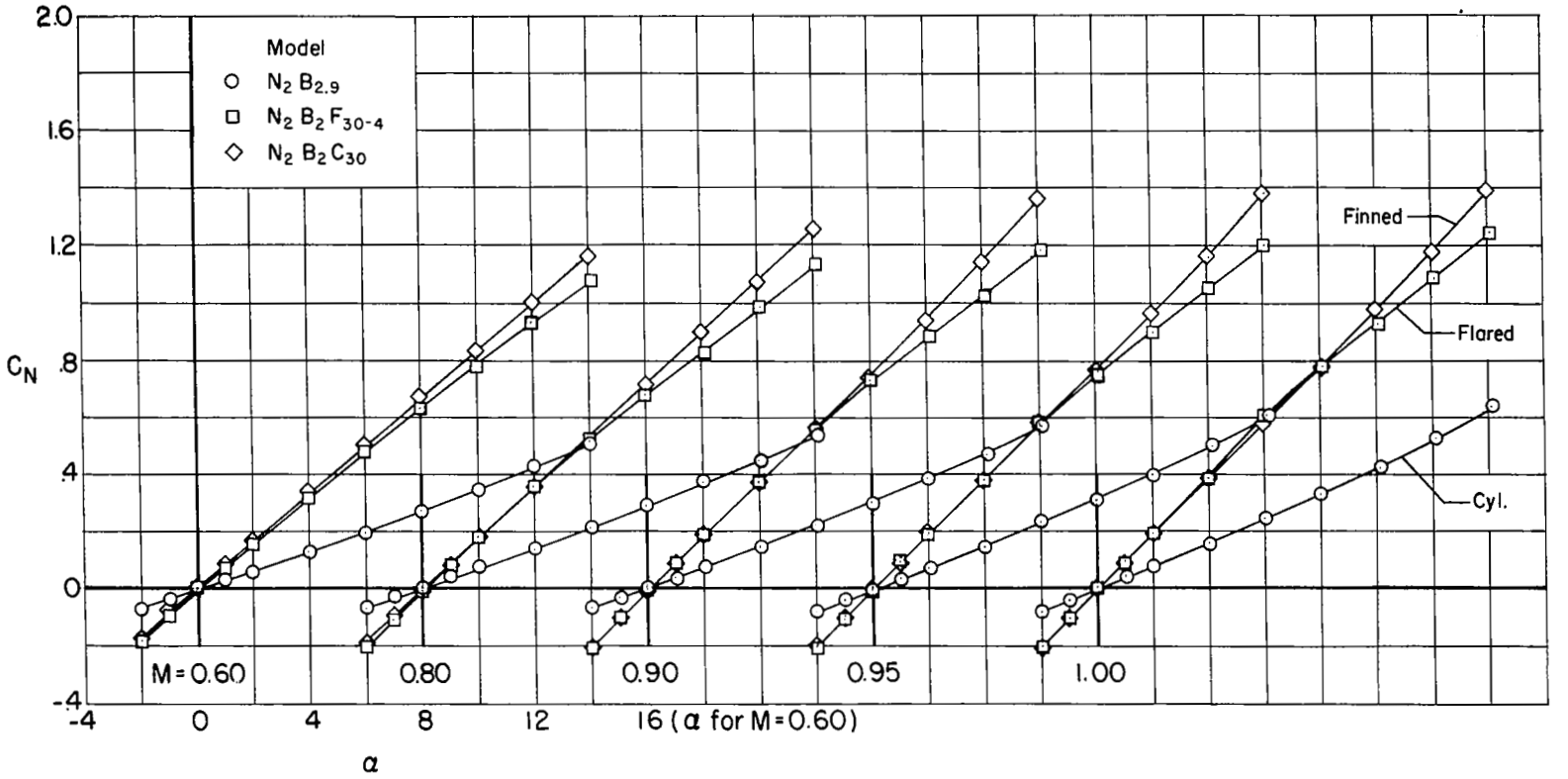

(a) M = 0.60 to 1.00

Figure 7.- Normal-force coefficients for models having flared or finned afterbody plan forms of 30° semivertex angle, or cylindrical afterbody.

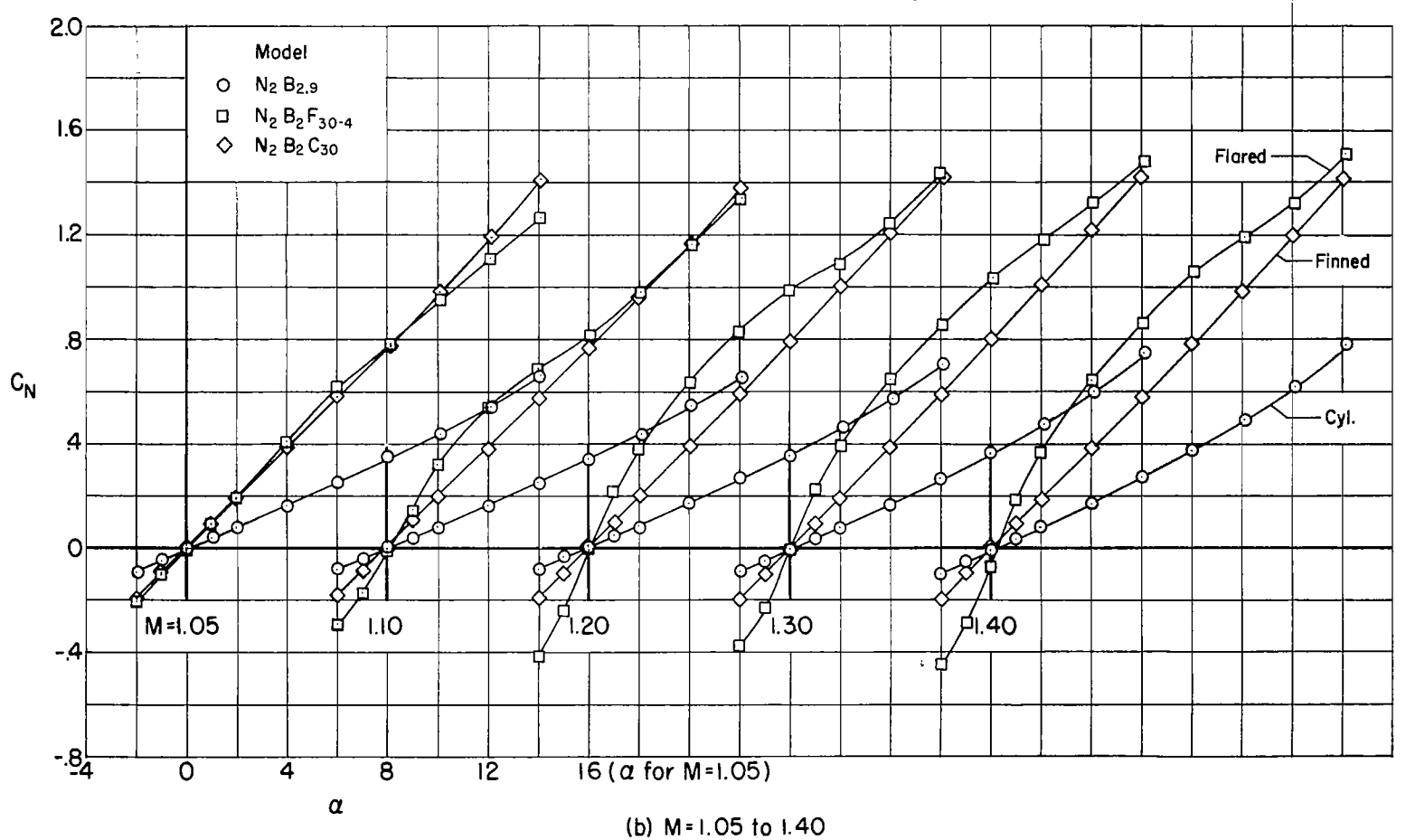

(b) M = 1.05 to 1.40

Figure 7.- Concluded.

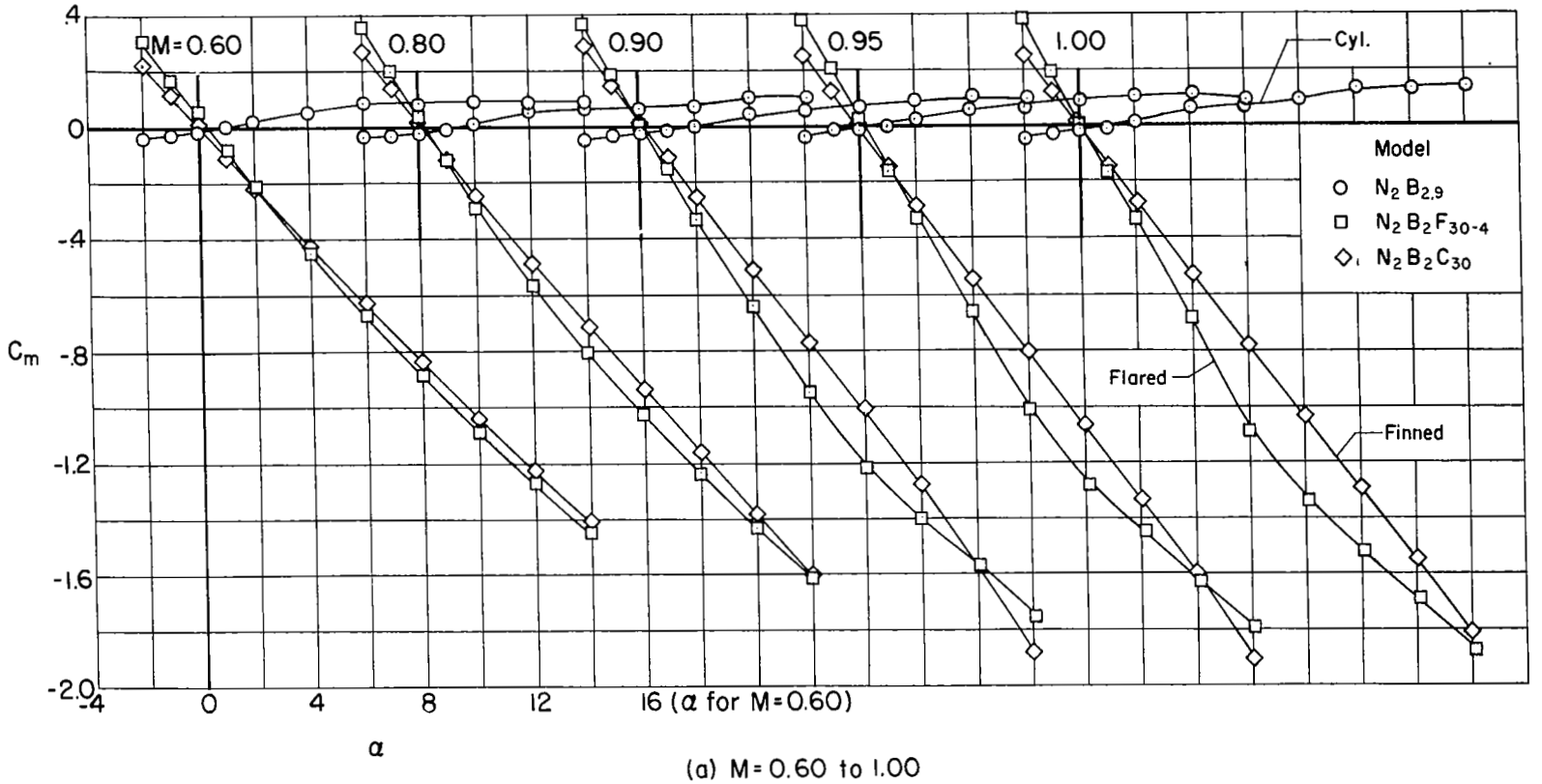

(a) M = 0.60 to 1.00

Figure 8.- Pitching-moment coefficients for models having flared or finned afterbody plan forms of 30° semivertex angle, or cylindrical afterbody.

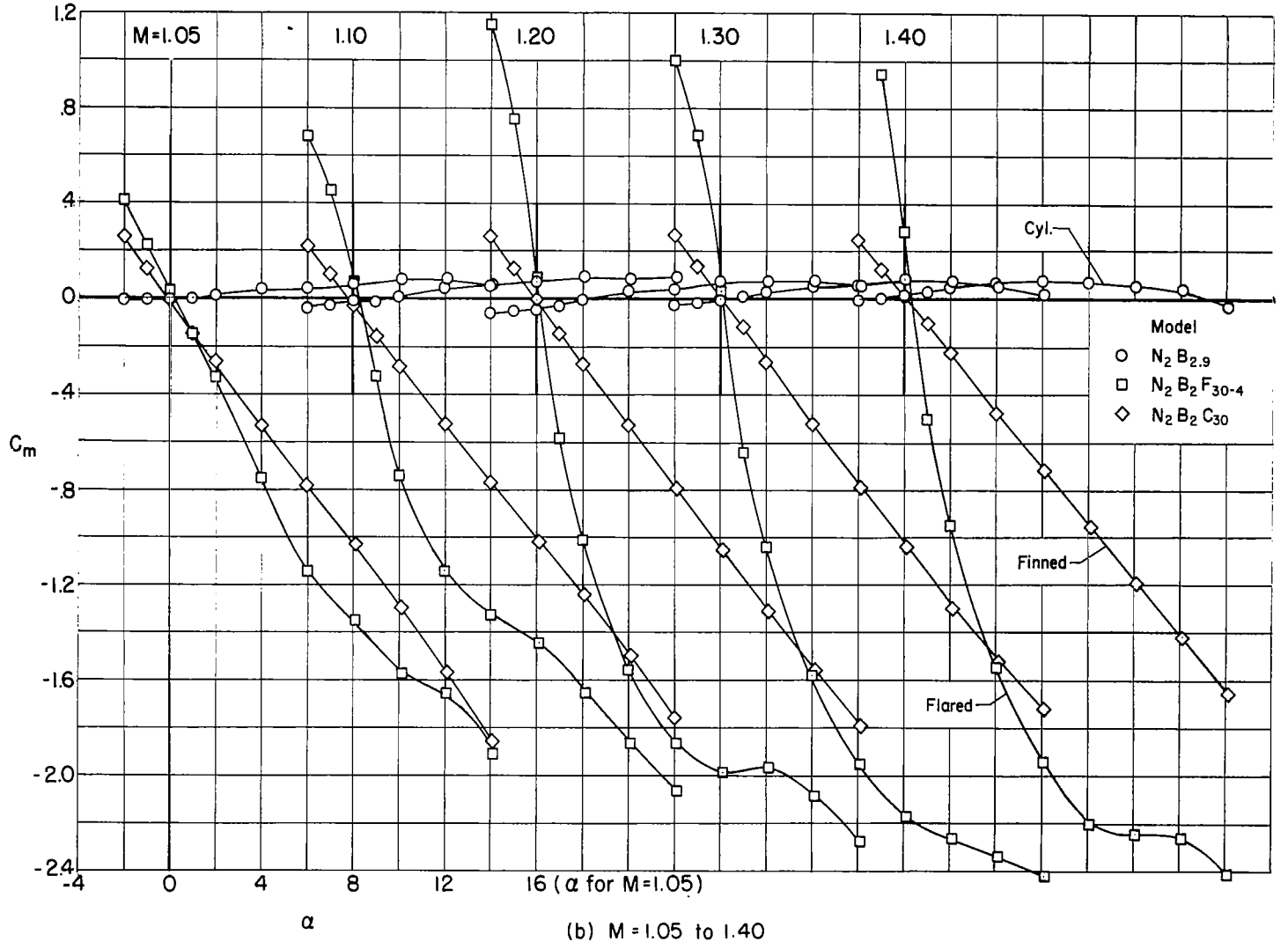

(b) M = 1.05 to 1.40

Figure 8.- Concluded.

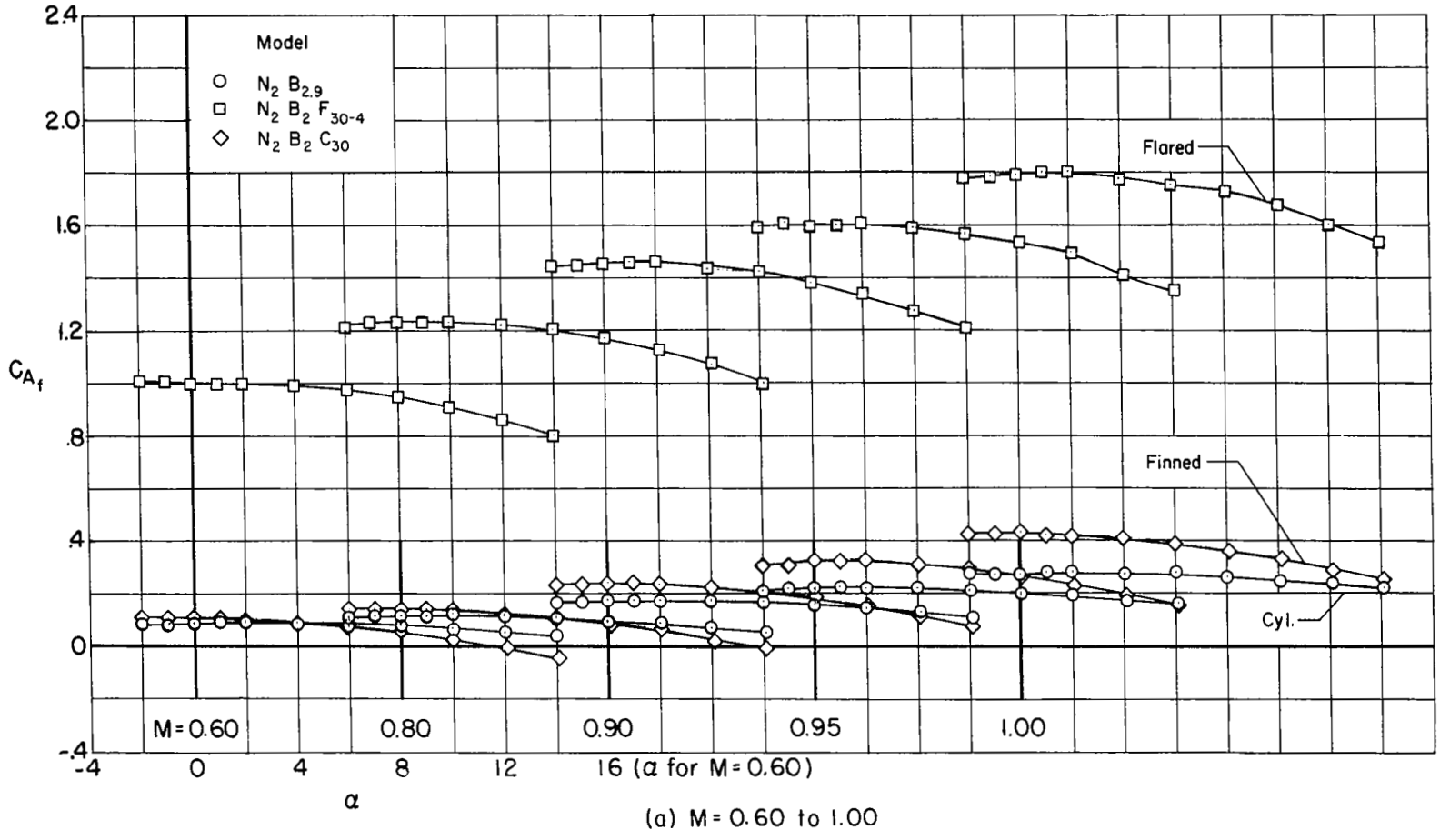

(a) M = 0.60 to 1.00

Figure 9.- Forebody axial-force coefficients for models having flared or finned afterbody plan forms of 30° semivertex angle, or cylindrical afterbody.

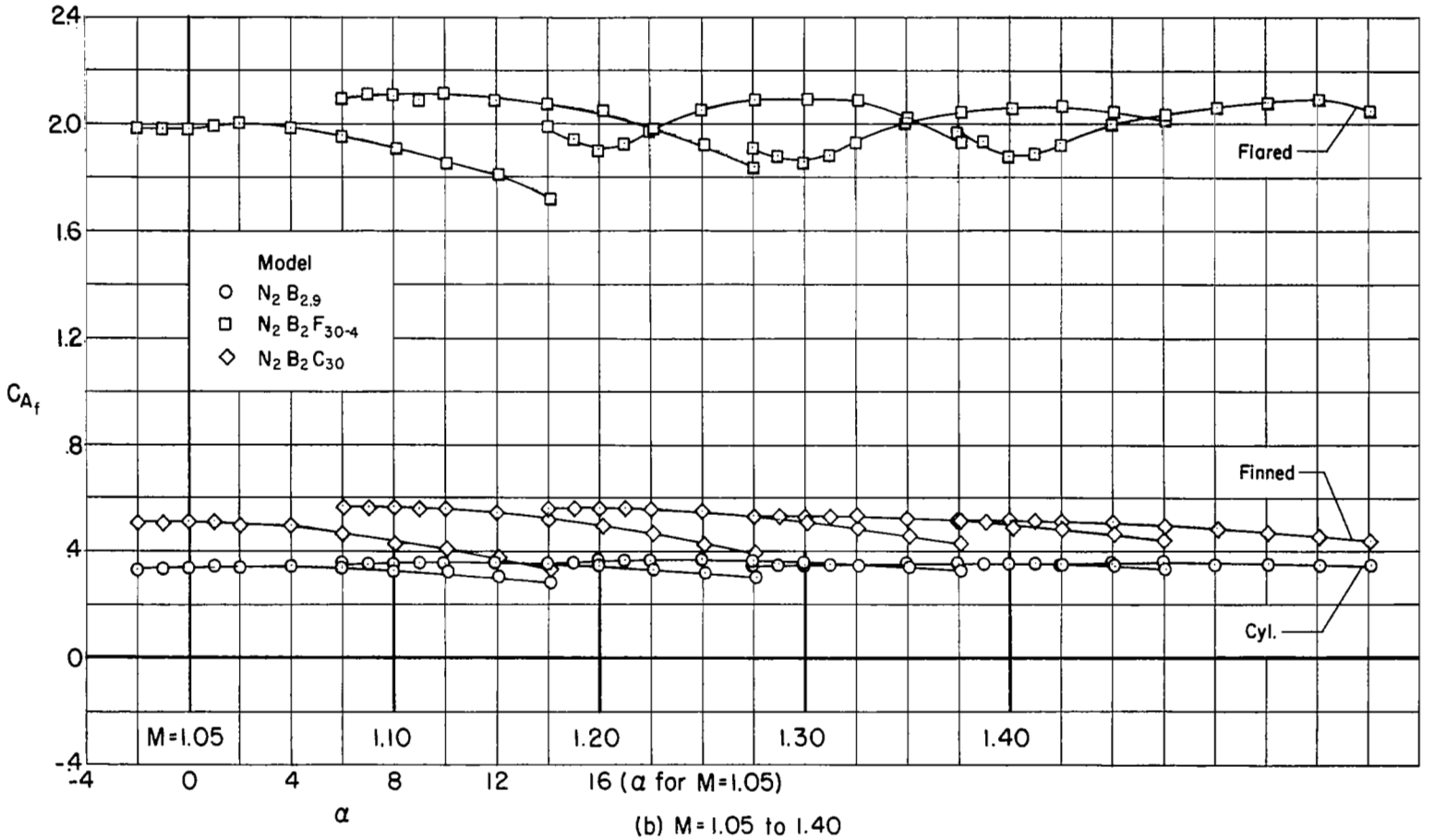

(b) M = 1.05 to 1.40

Figure 9.- Concluded.

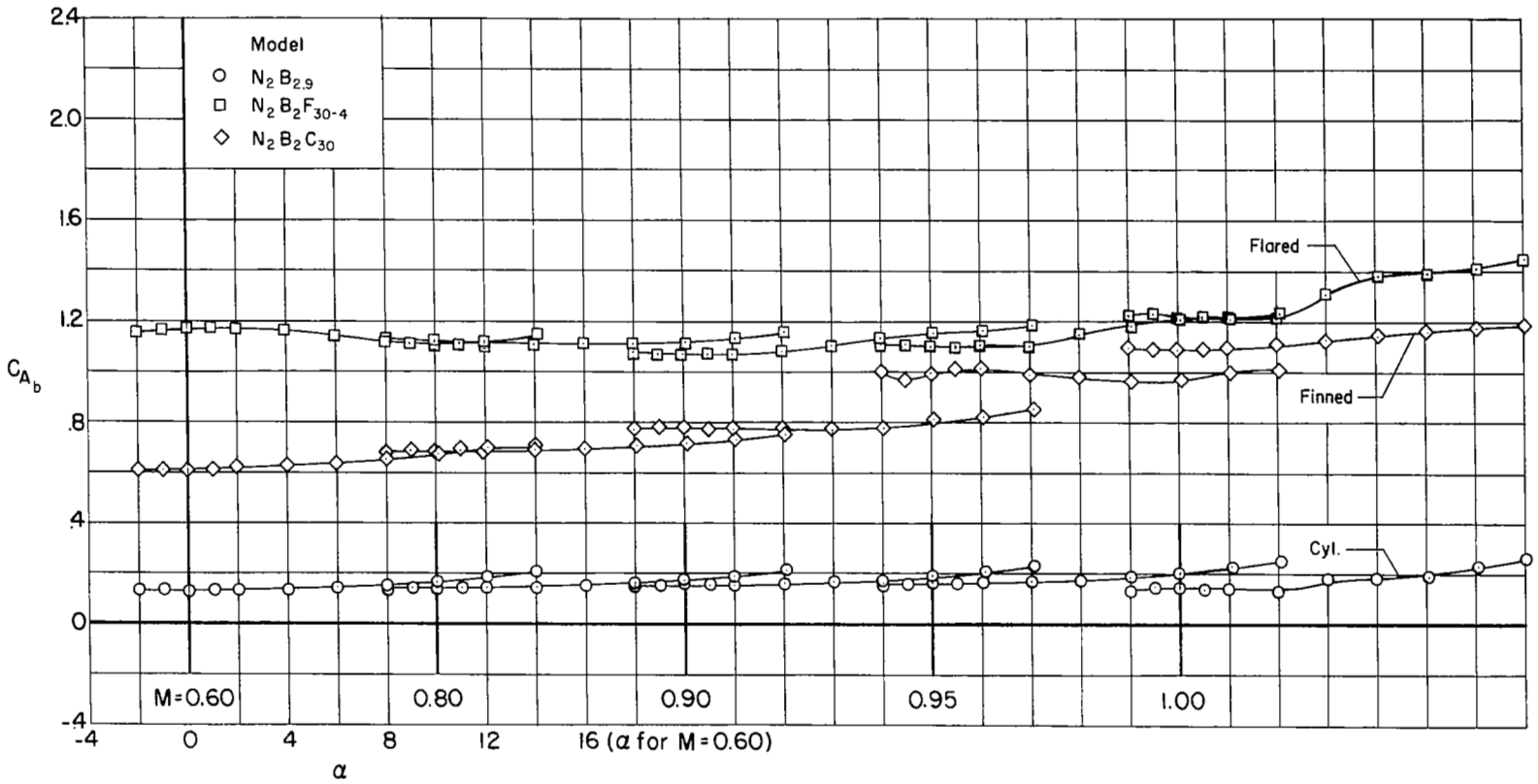

(a) M = 0.60 to 1.00

Figure 10.- Base axial-force coefficients for models having flared or finned afterbody plan forms of 30° semivertex angle, or cylindrical afterbody.

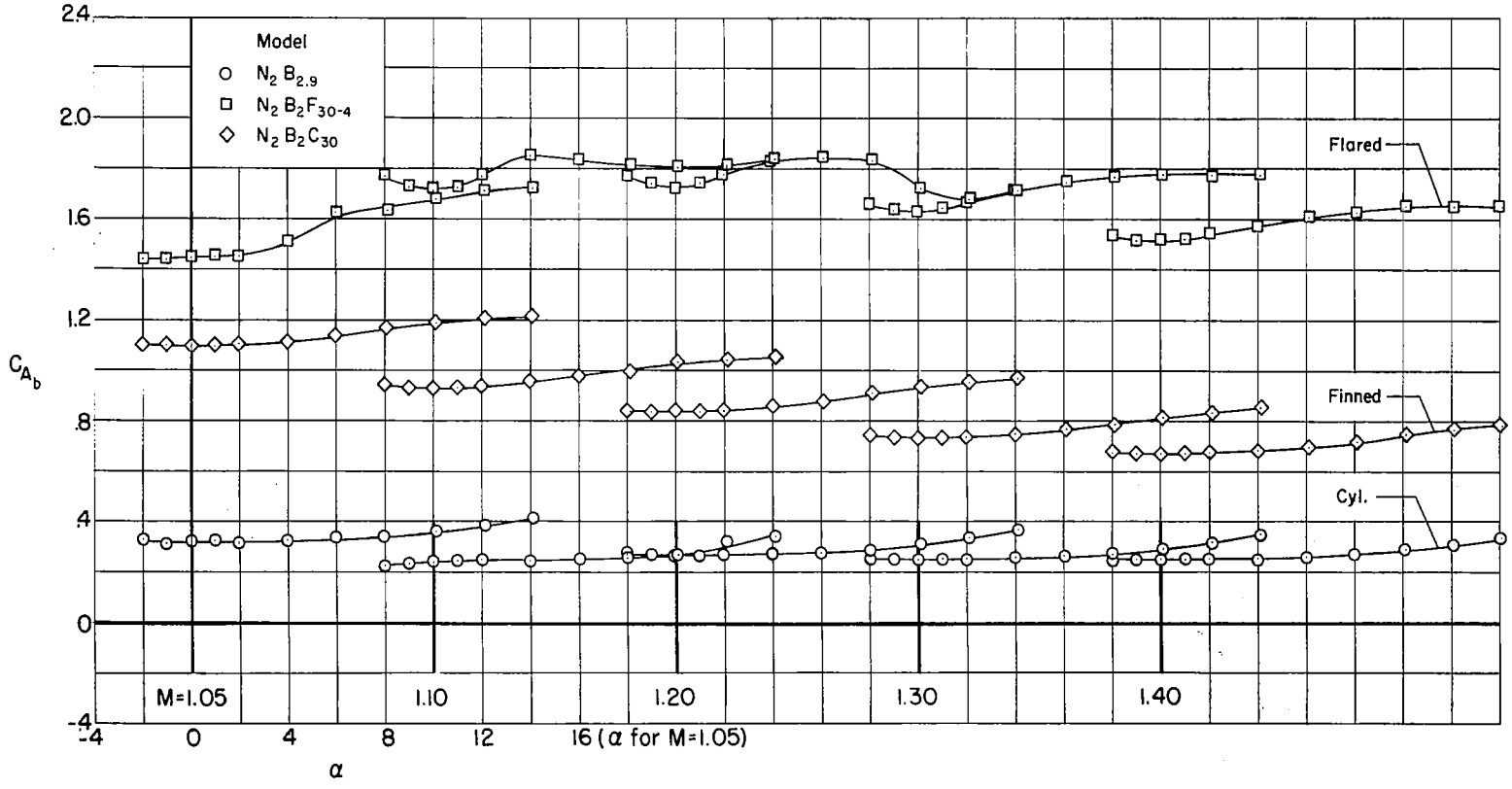

(b) M=1.05 to 1.40

Figure 10.- Concluded.

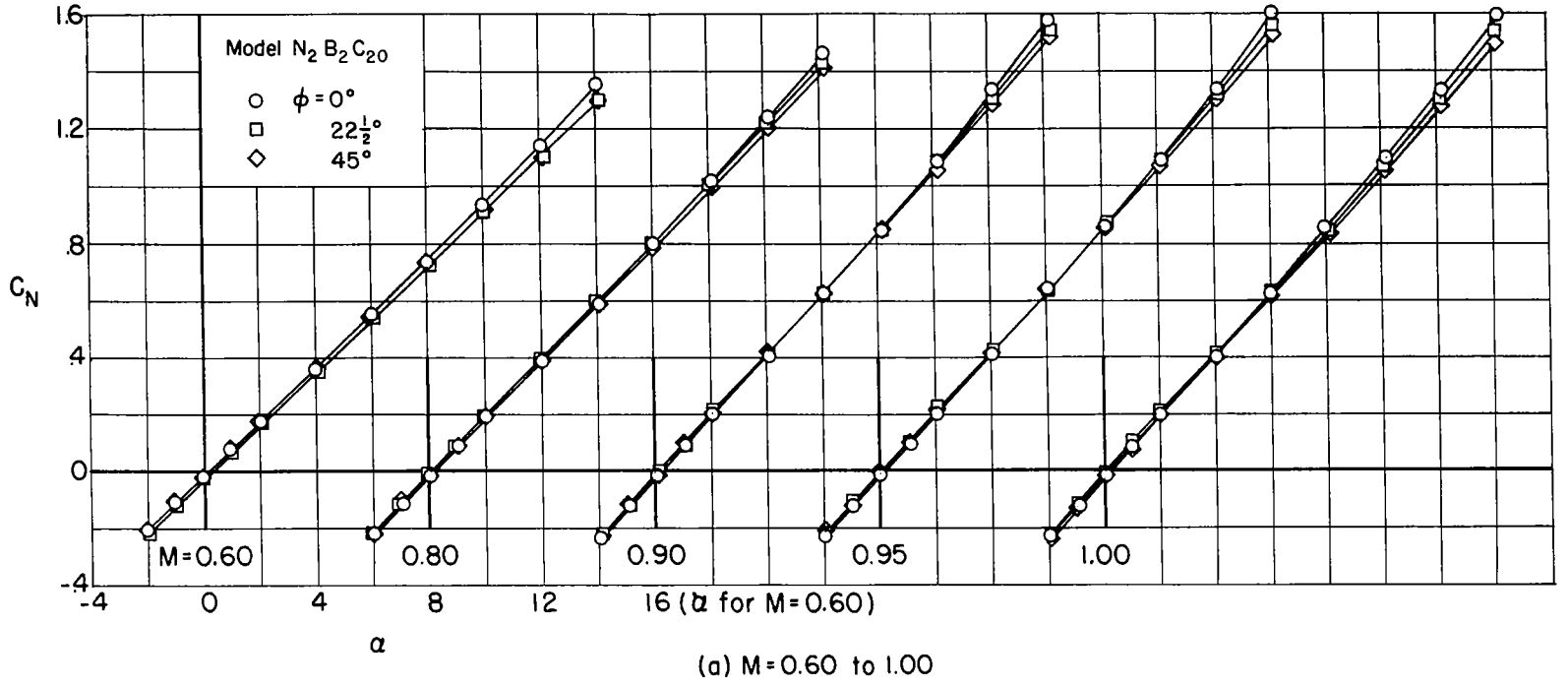

(a) M = 0.60 to 1.00

Figure 11.- Effects of roll angle on the normal-force characteristics of the model having fins of 20° semivertex angle.

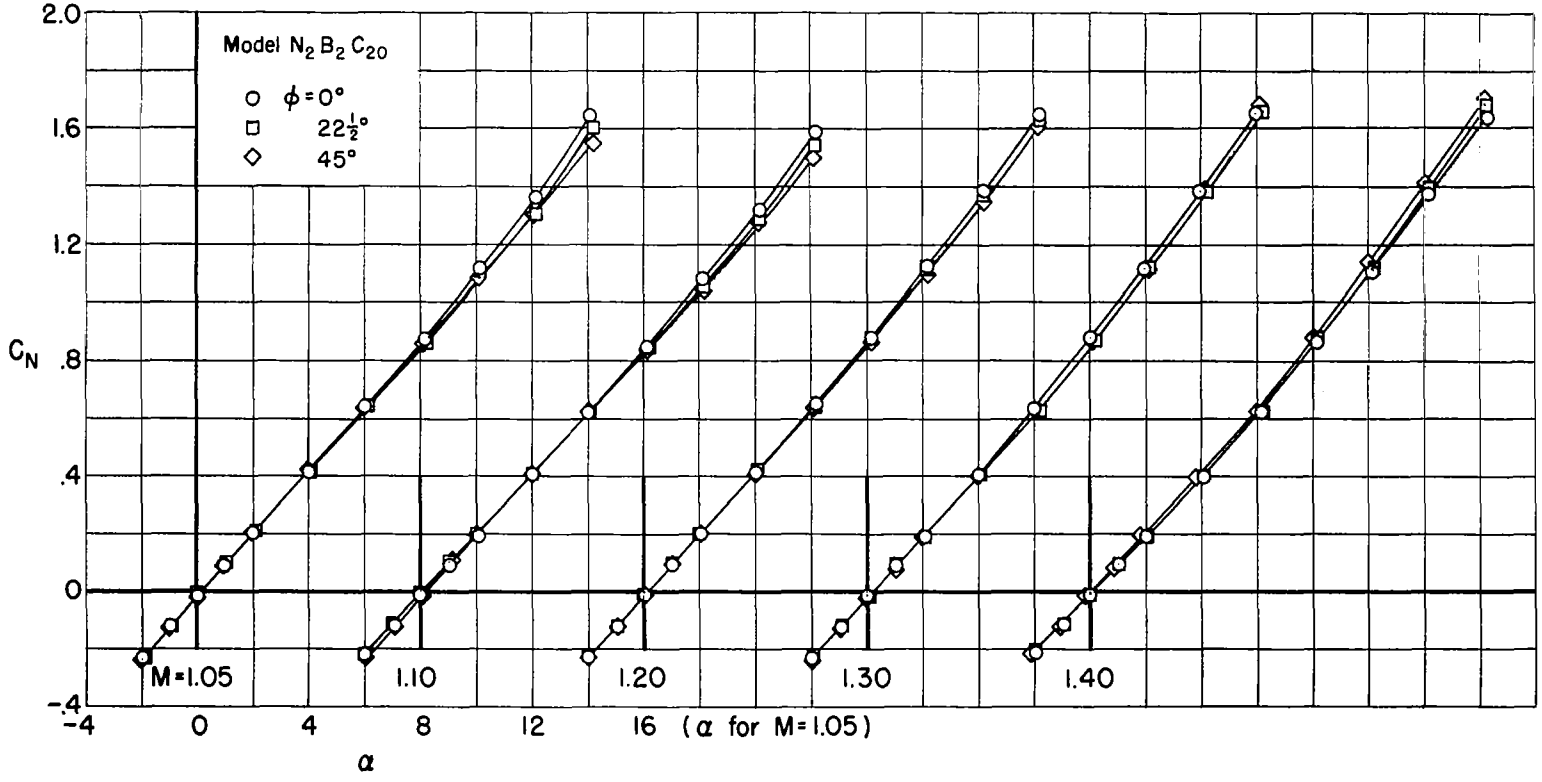

(b) M = 1.05 to 1.40

Figure 11.- Concluded.

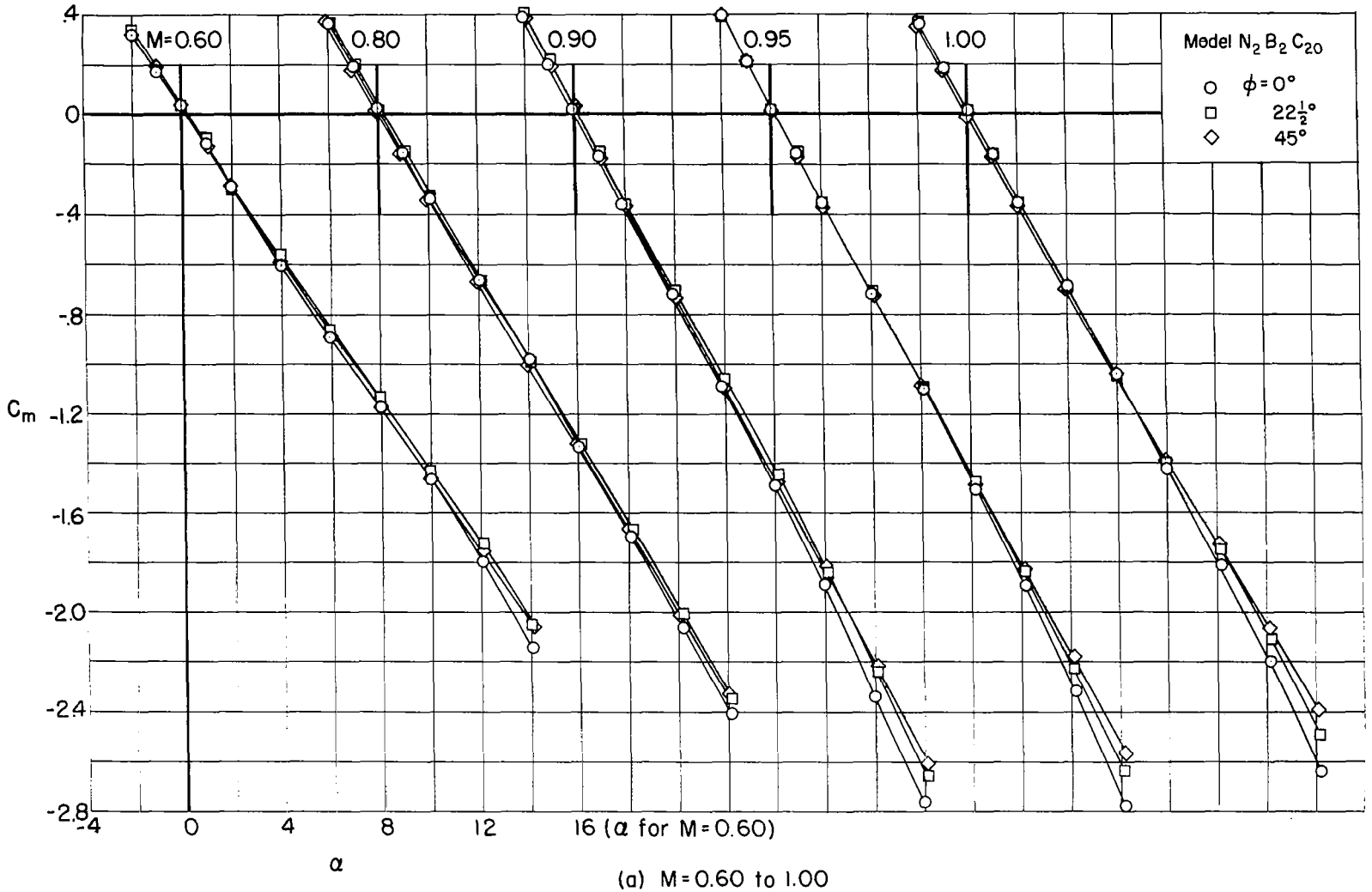

(a) M = 0.60 to 1.00

Figure 12.- Effects of roll angle on the pitching-moment characteristics of the model having fins of 20° semivertex angle.

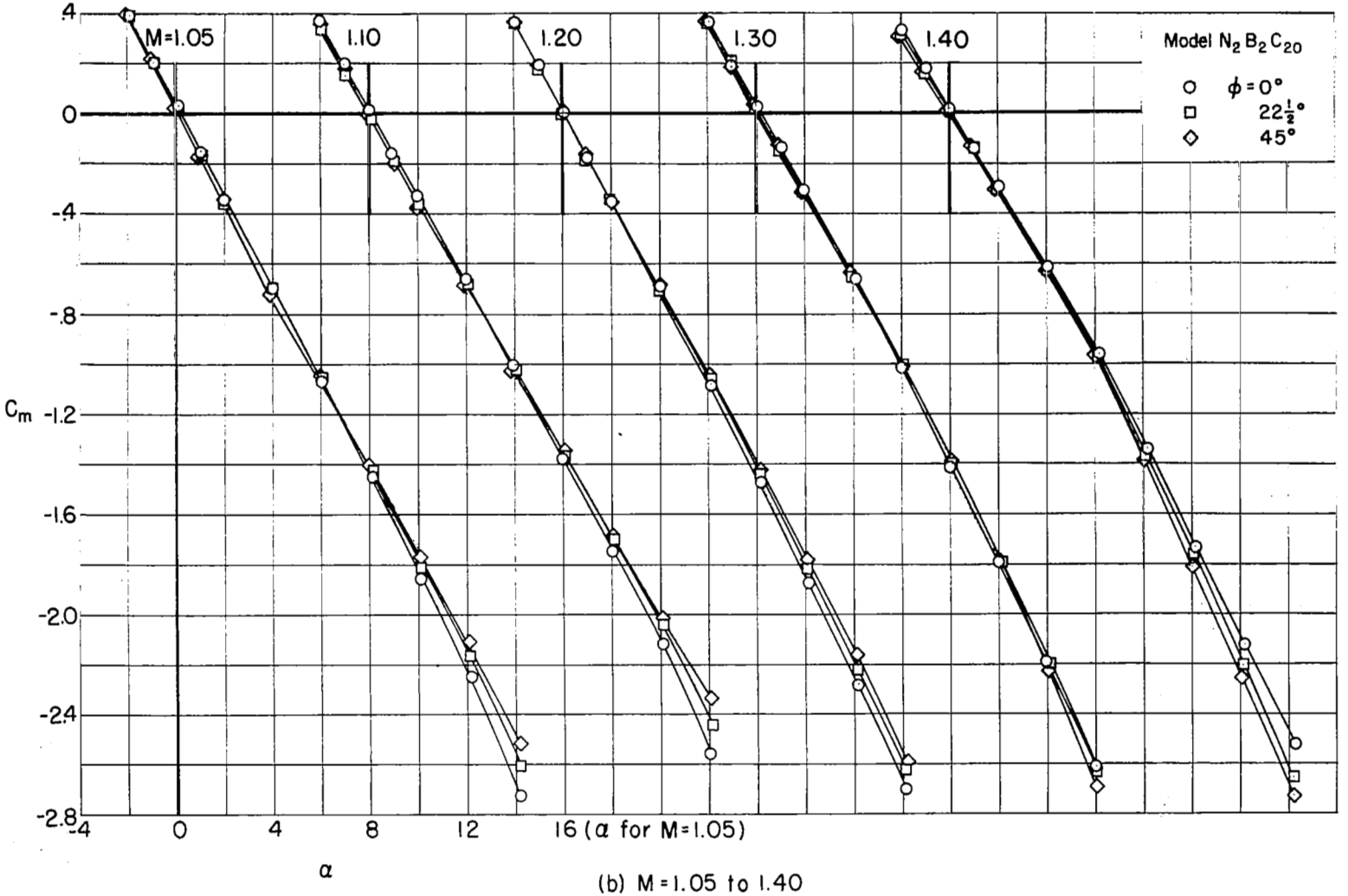

(b) M = 1.05 to 1.40

Figure 12.- Concluded.

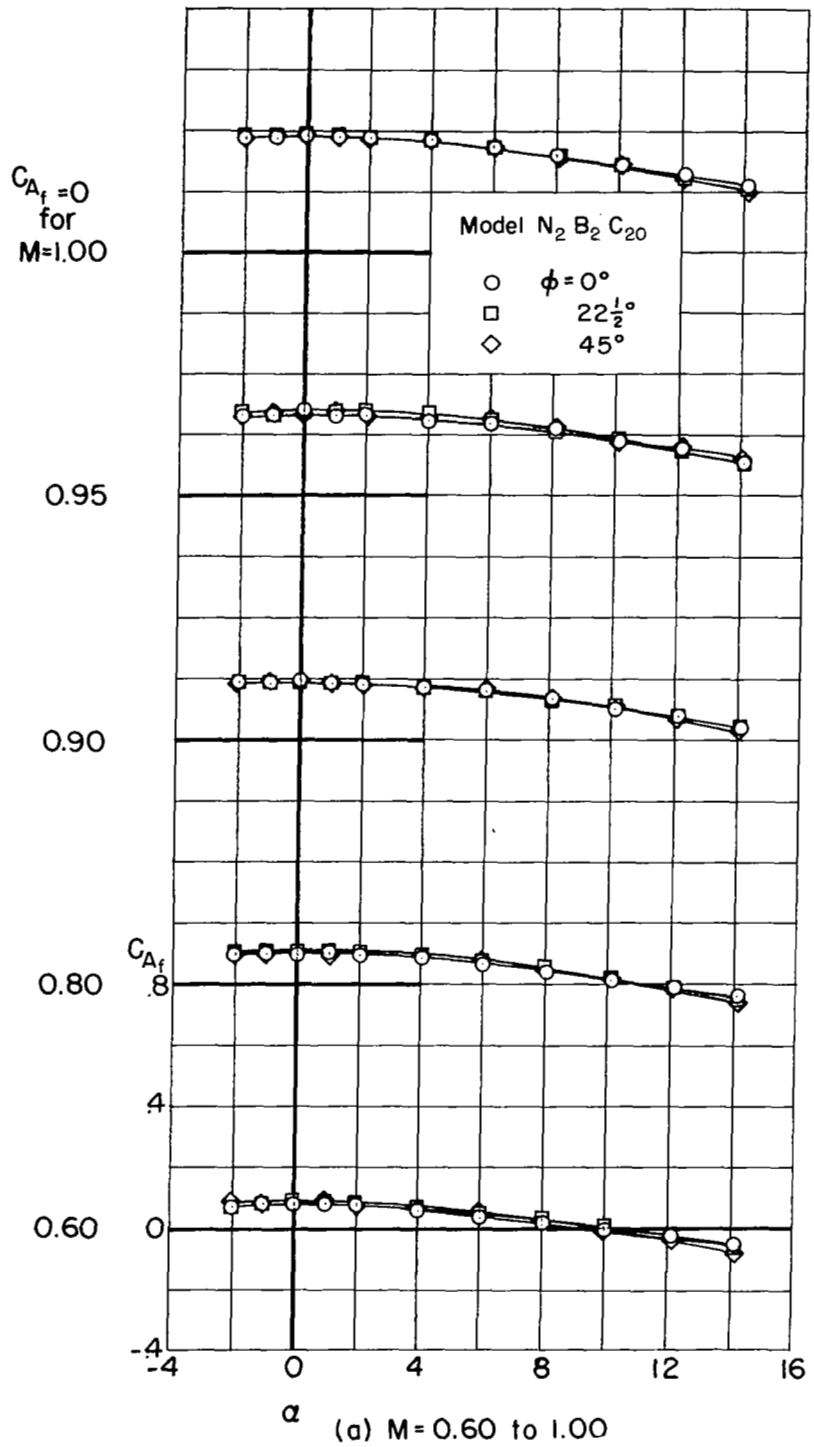

Figure 13.- Effects of roll angle on the forebody axial-force characteristics of the model having fins of 20° semivertex angle.

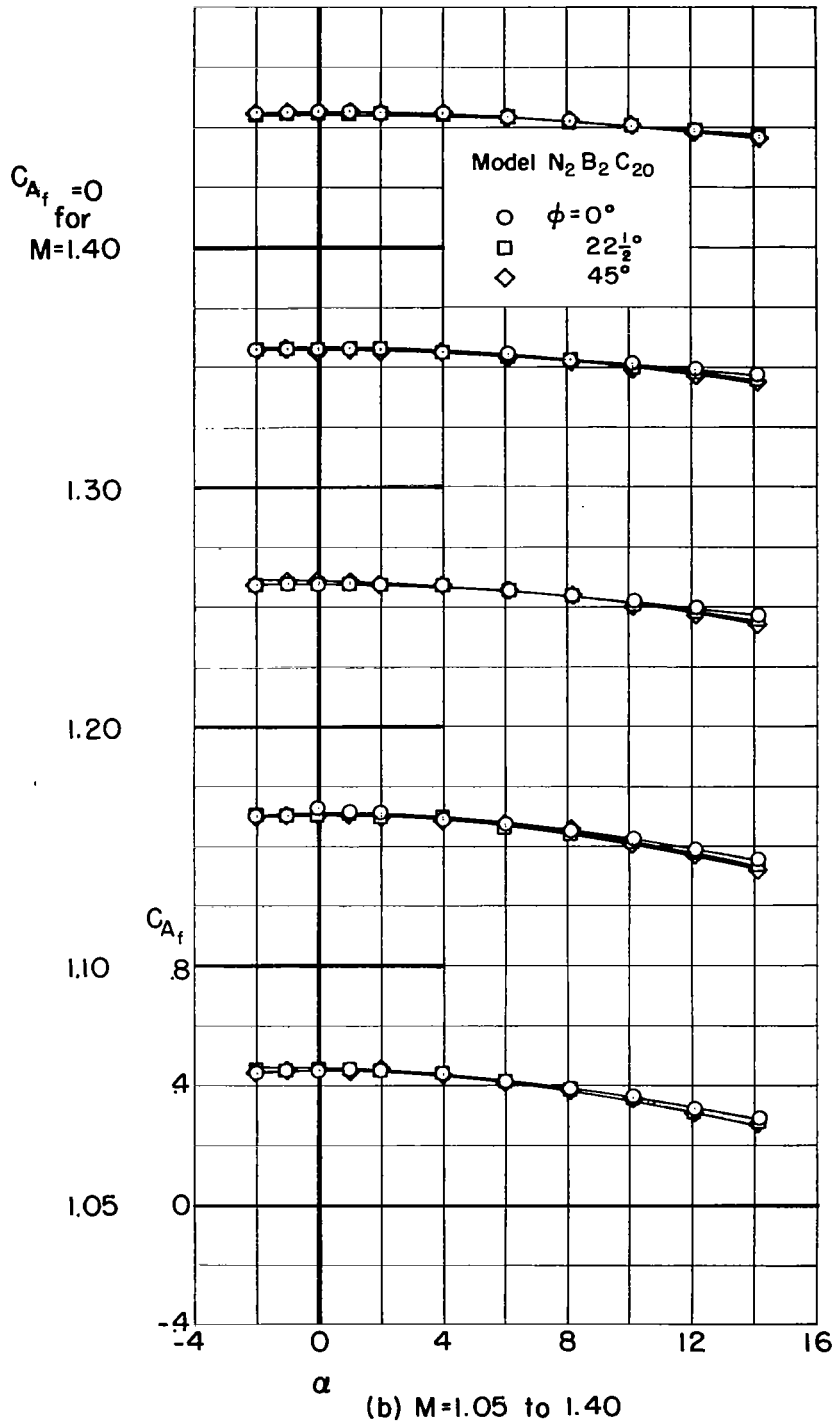

(b) M=1.05 to 1.40

Figure 13.- Concluded.

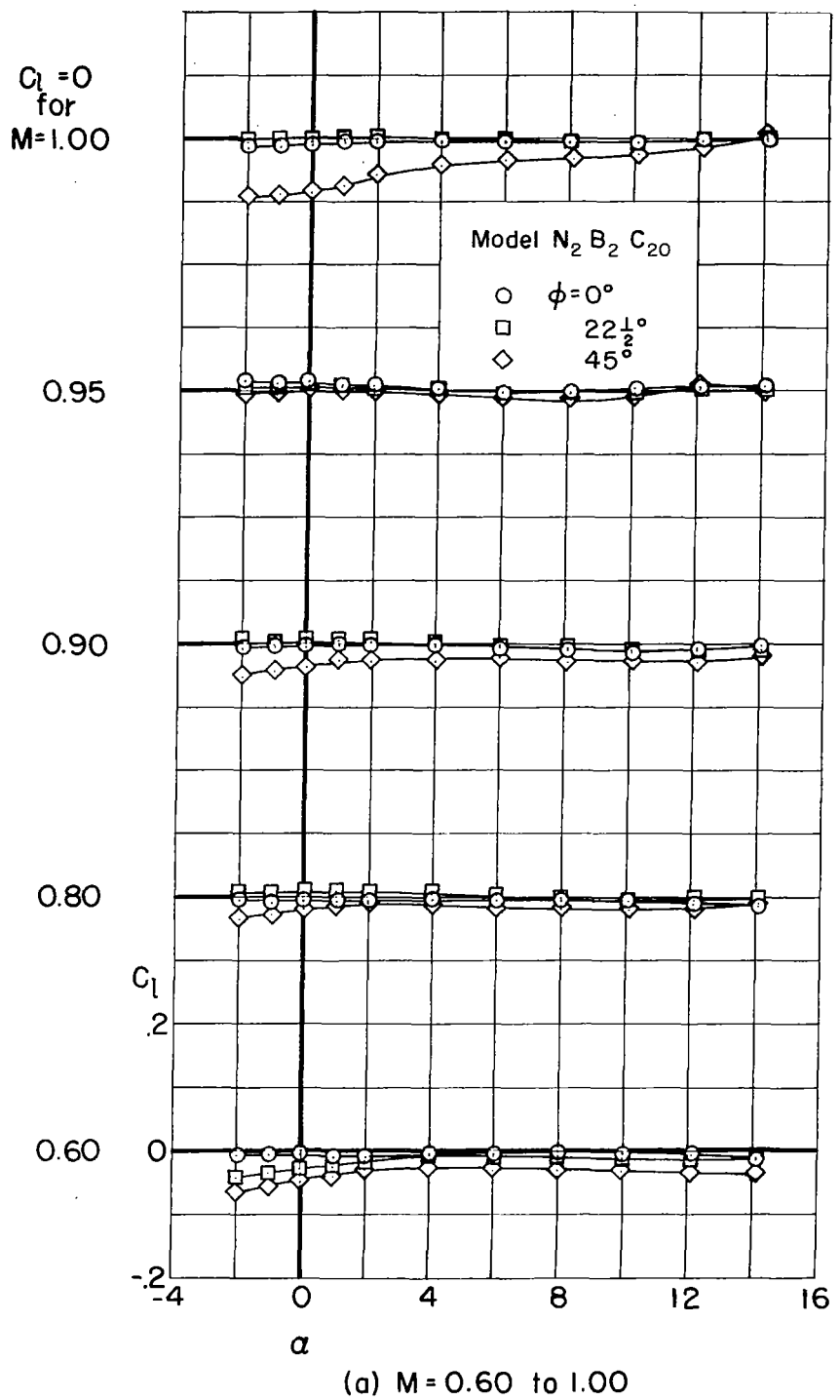

(a) M = 0.60 to 1.00

Figure 14.- Effects of roll angle on the rolling-moment characteristics of the model having fins of 20° semivertex angle.

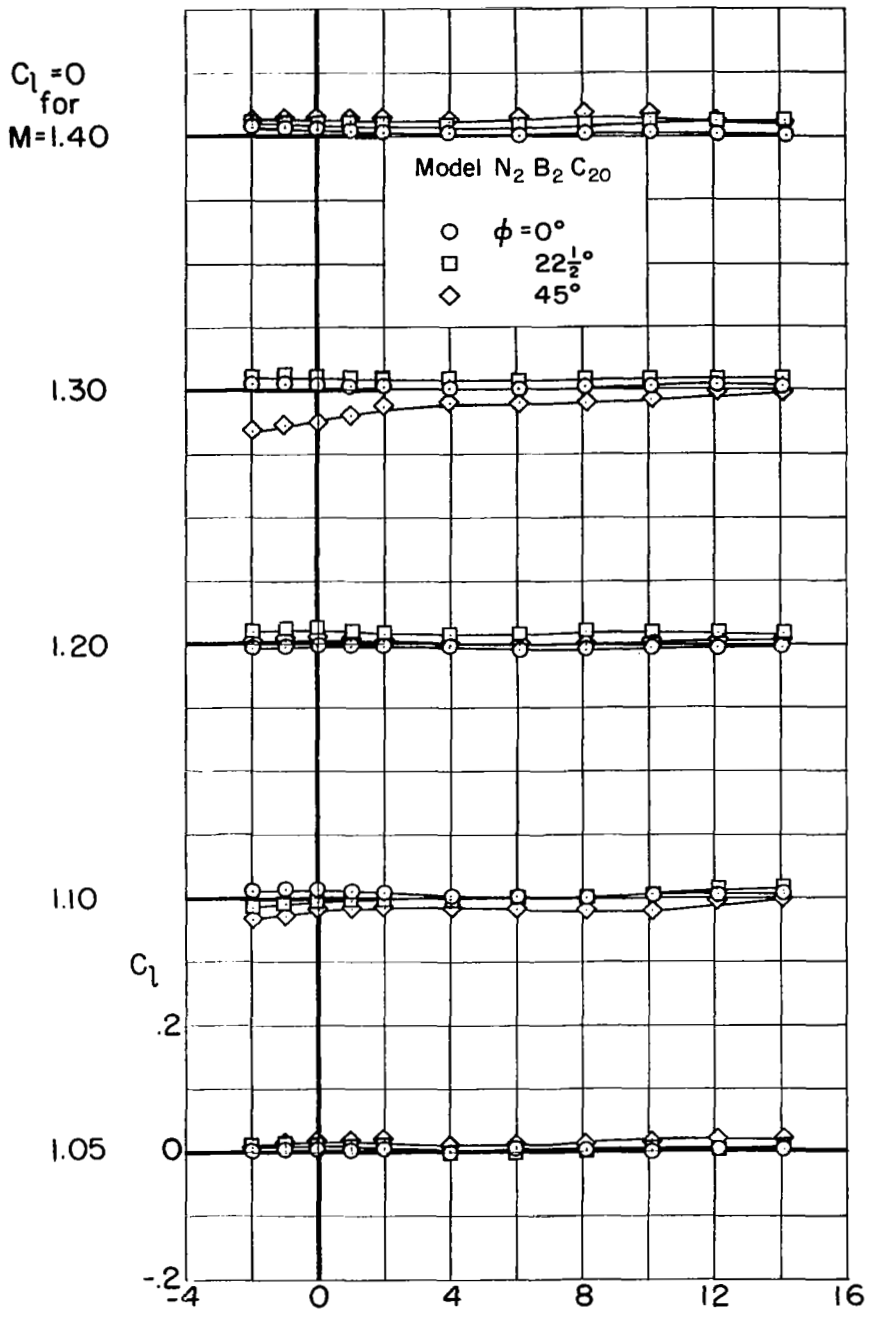

(b) M=1.05 to 1.40

Figure 14.- Concluded.

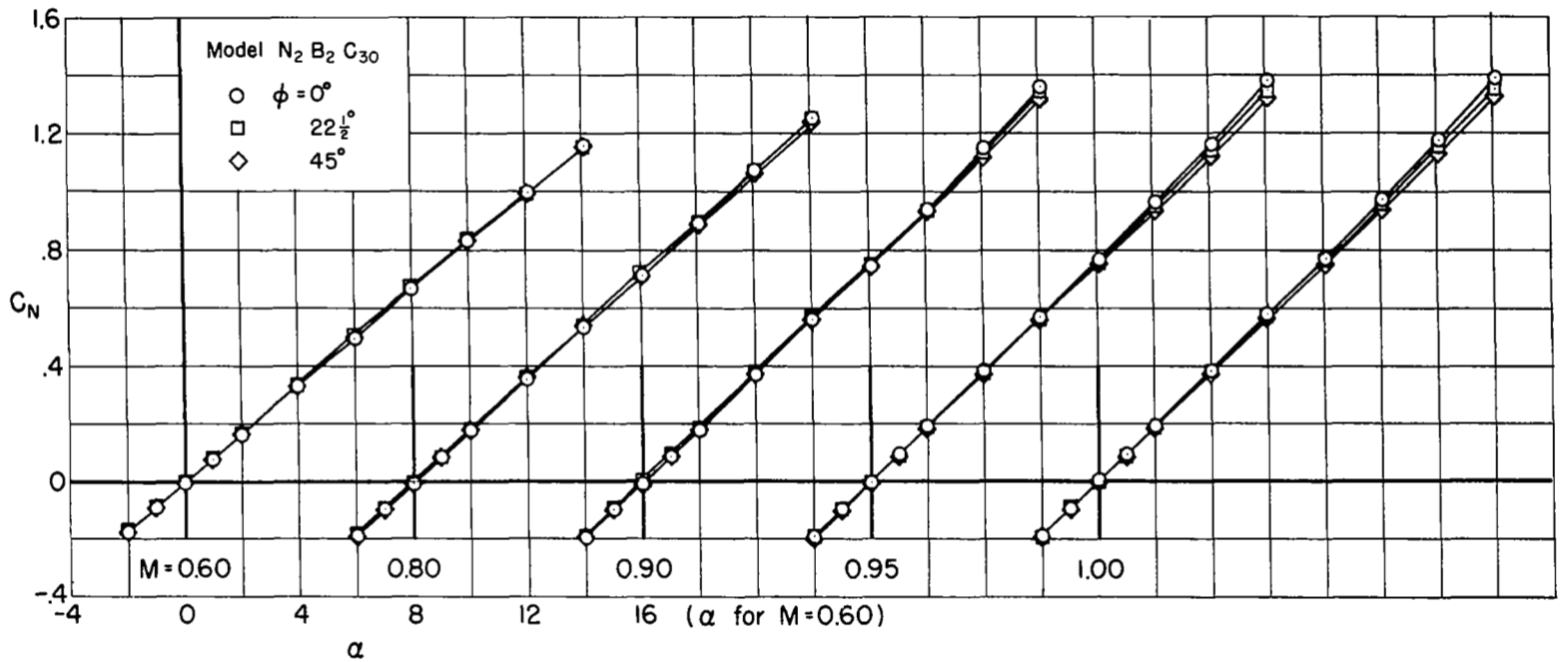

(a) M = 0.60 to 1.00

Figure 15.- Effects of roll angle on the normal-force characteristics of the model having fins of 30° semivertex angle.

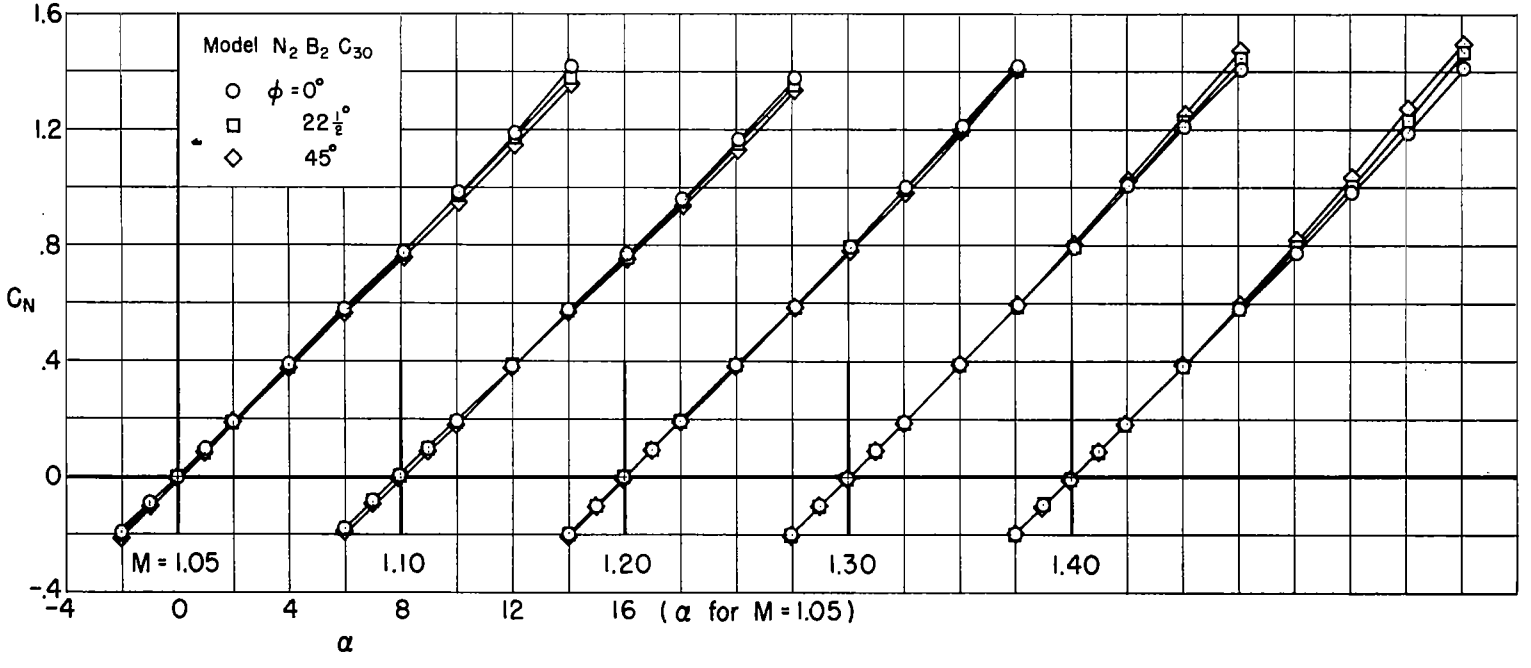

(b) M = 1.05 to 1.40

Figure 15.- Concluded.

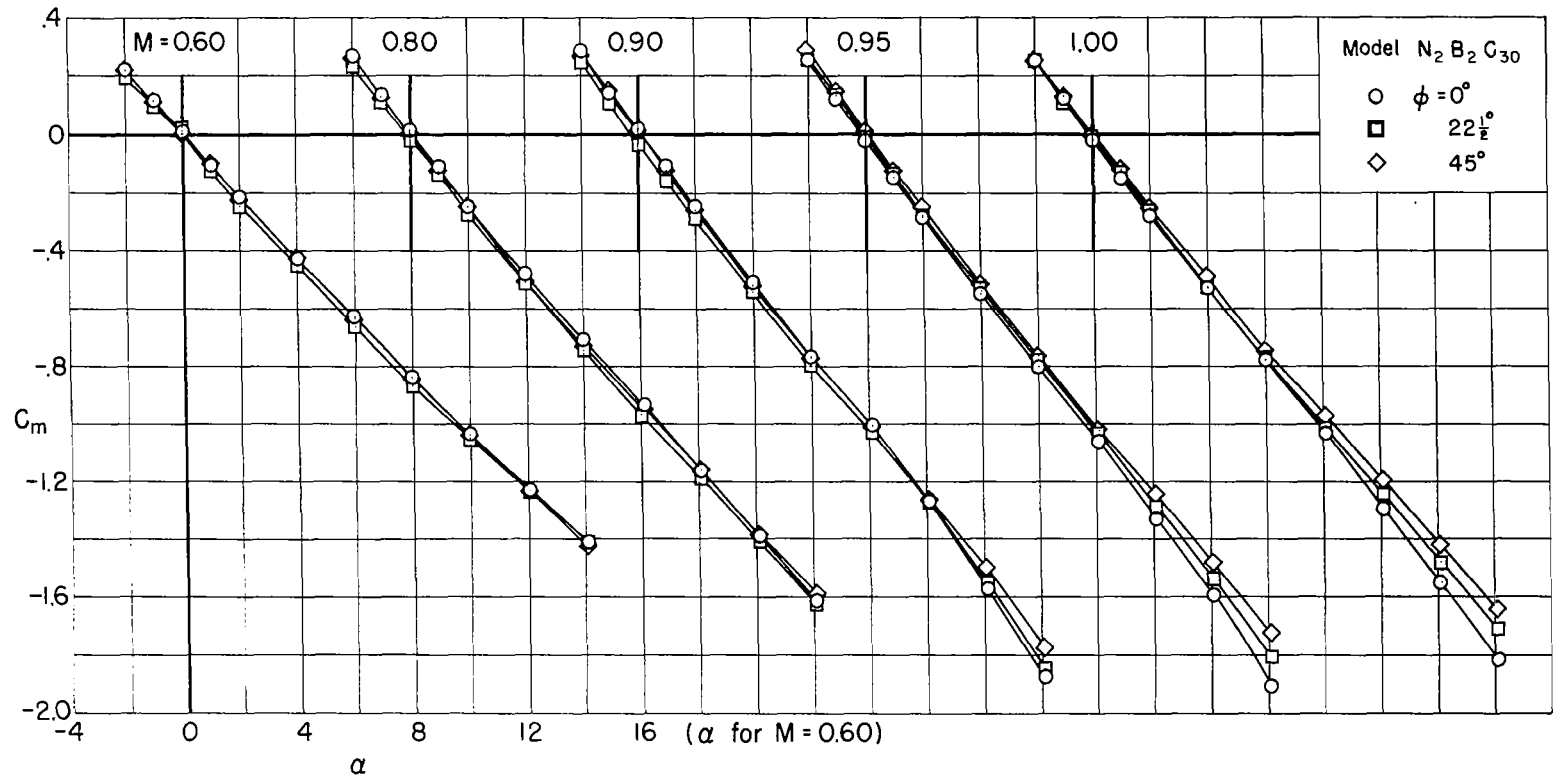

(a) M = 0.60 to 1.00

Figure 16.- Effects of roll angle on the pitching-moment characteristics of the model having fins of 30° semivertex angle.

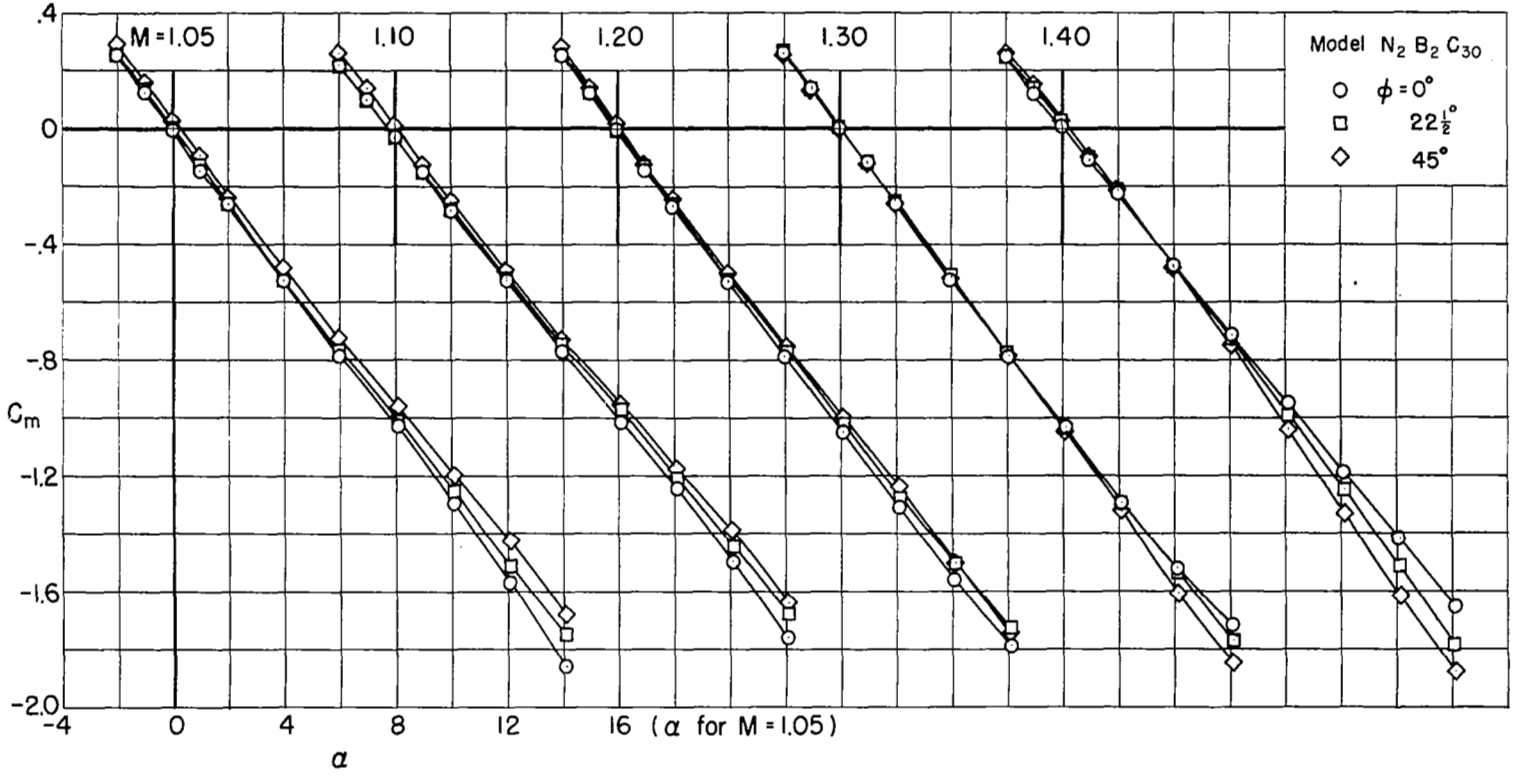

(b) M = 1.05 to 1.40

Figure 16.- Concluded.

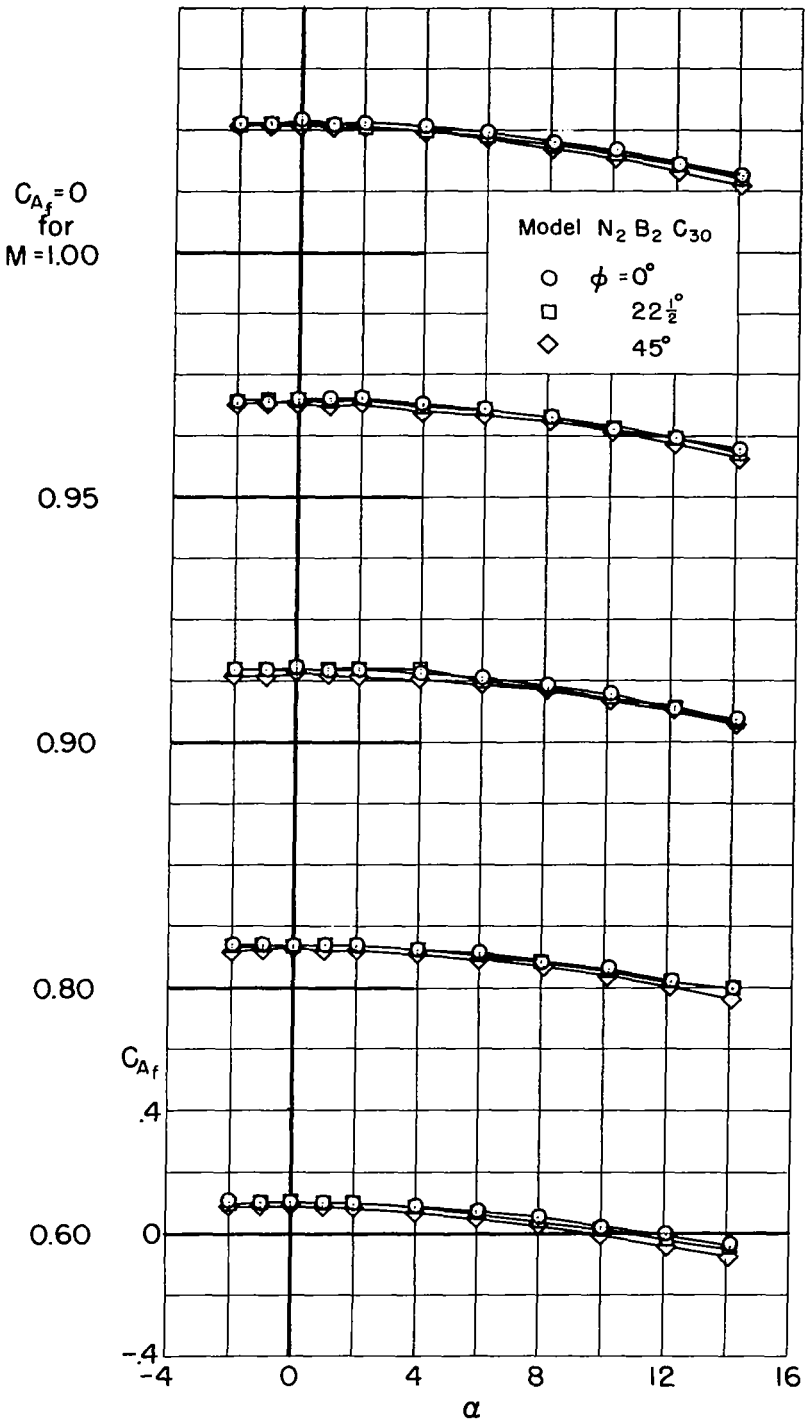

(a) M = 0.60 to 1.00

Figure 17.- Effects of roll angle on the forebody axial-force characteristics of the model having fins of 30° semivertex angle.

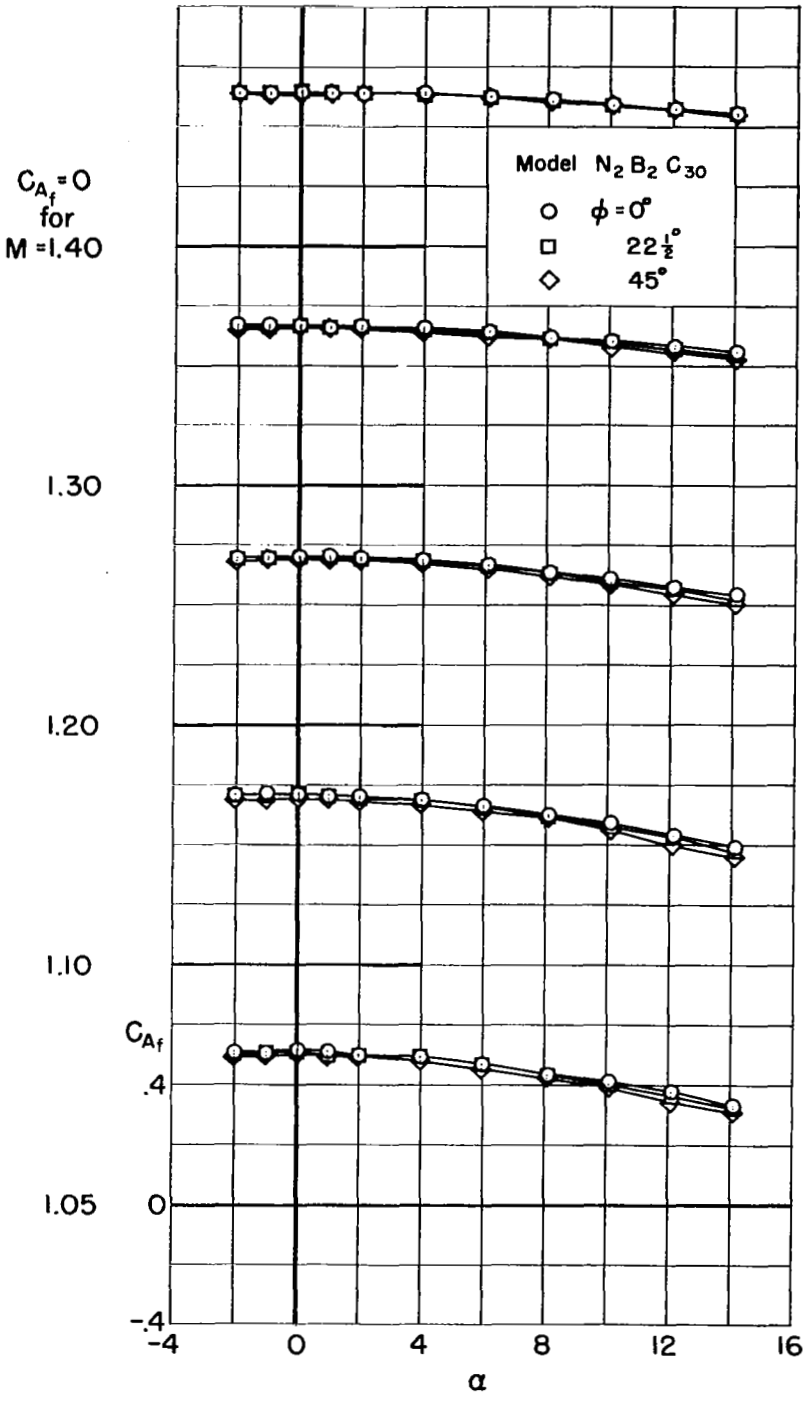

(b) M = 1.05 to 1.40

Figure 17.- Concluded.

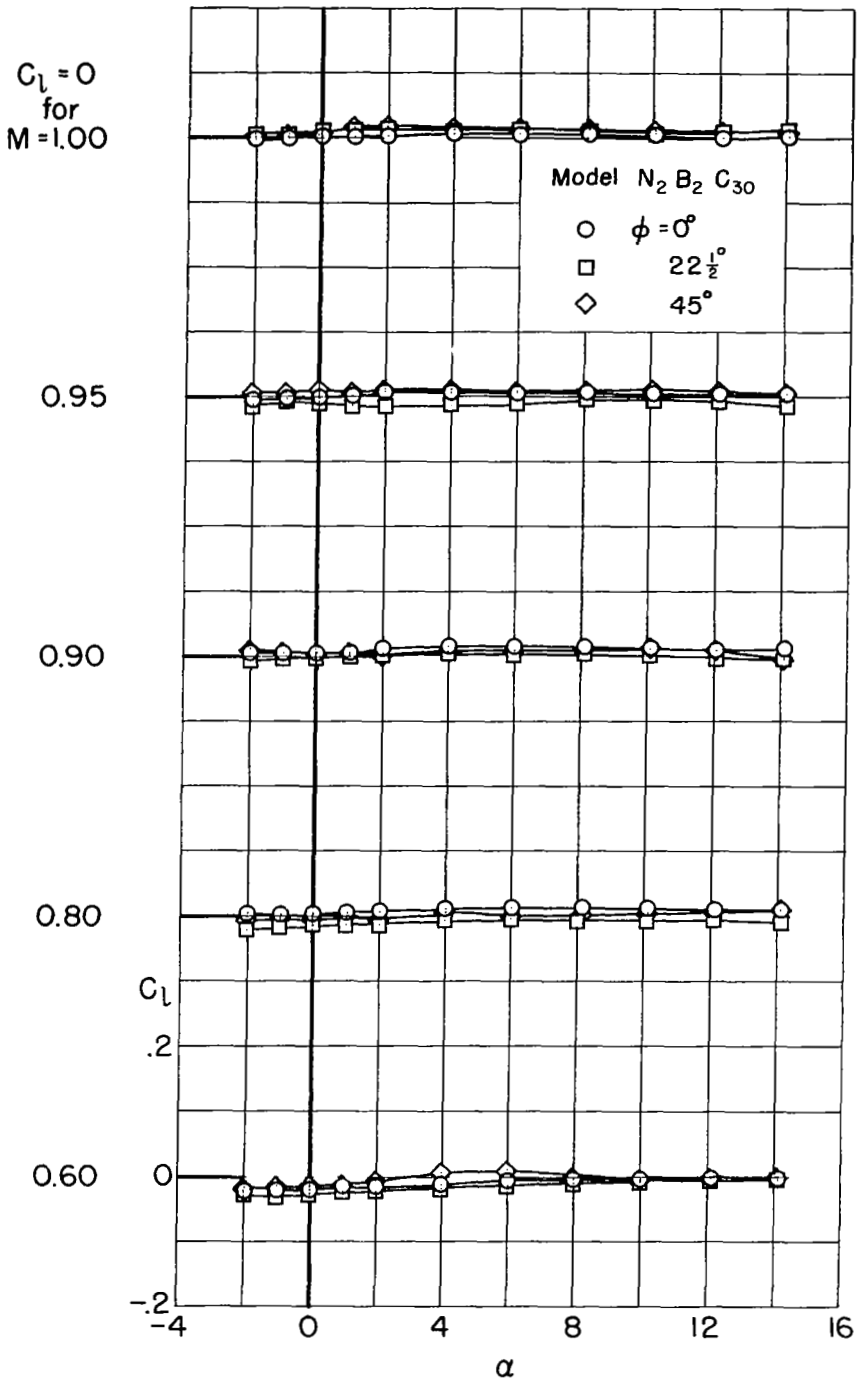

(a) M = 0.60 to 1.00

Figure 18.- Effects of roll angle on the rolling-moment characteristics of the model having fins of 30° semivertex angle.

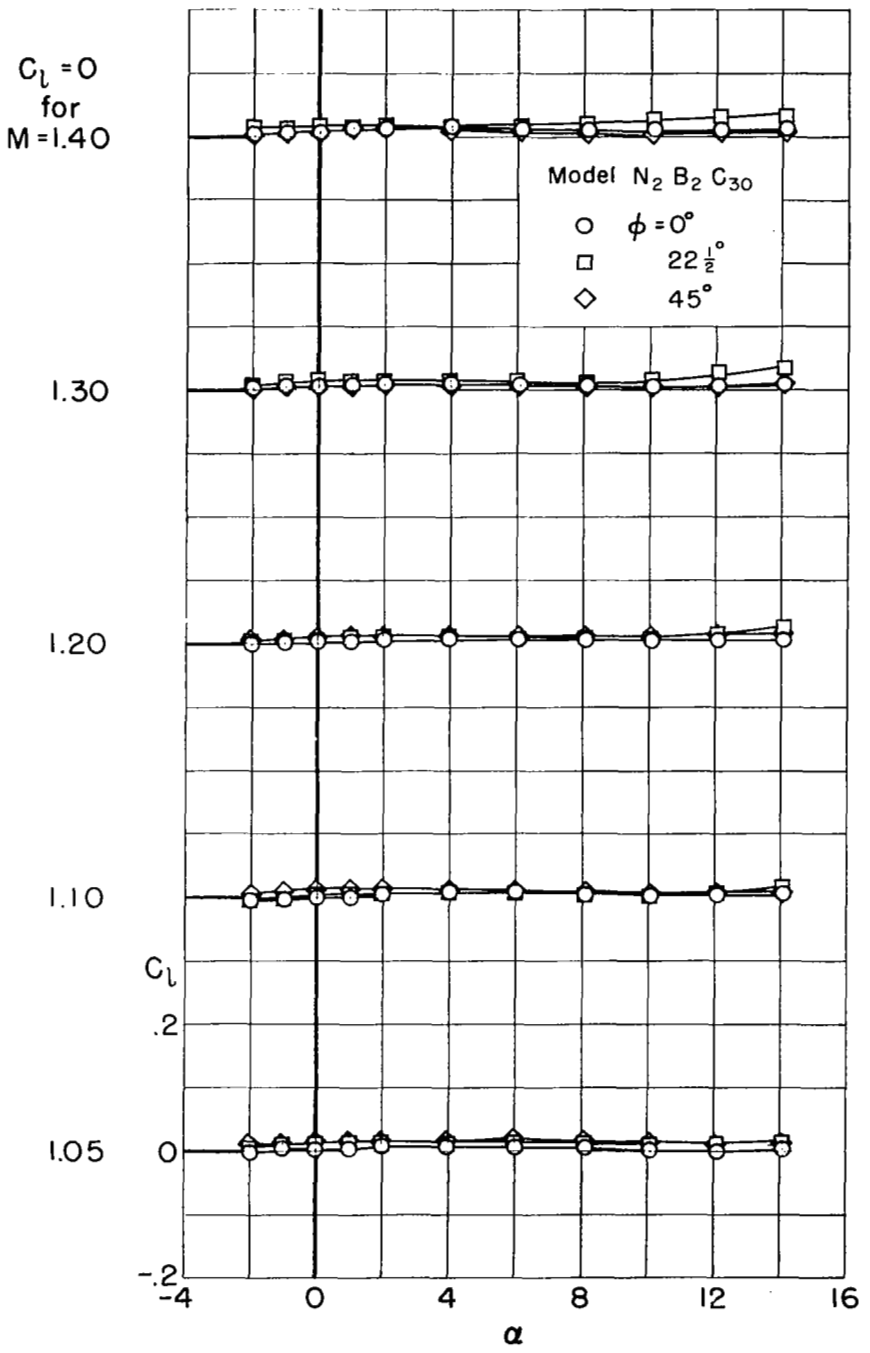

(b) M = 1.05 to 1.40

Figure 18.- Concluded.

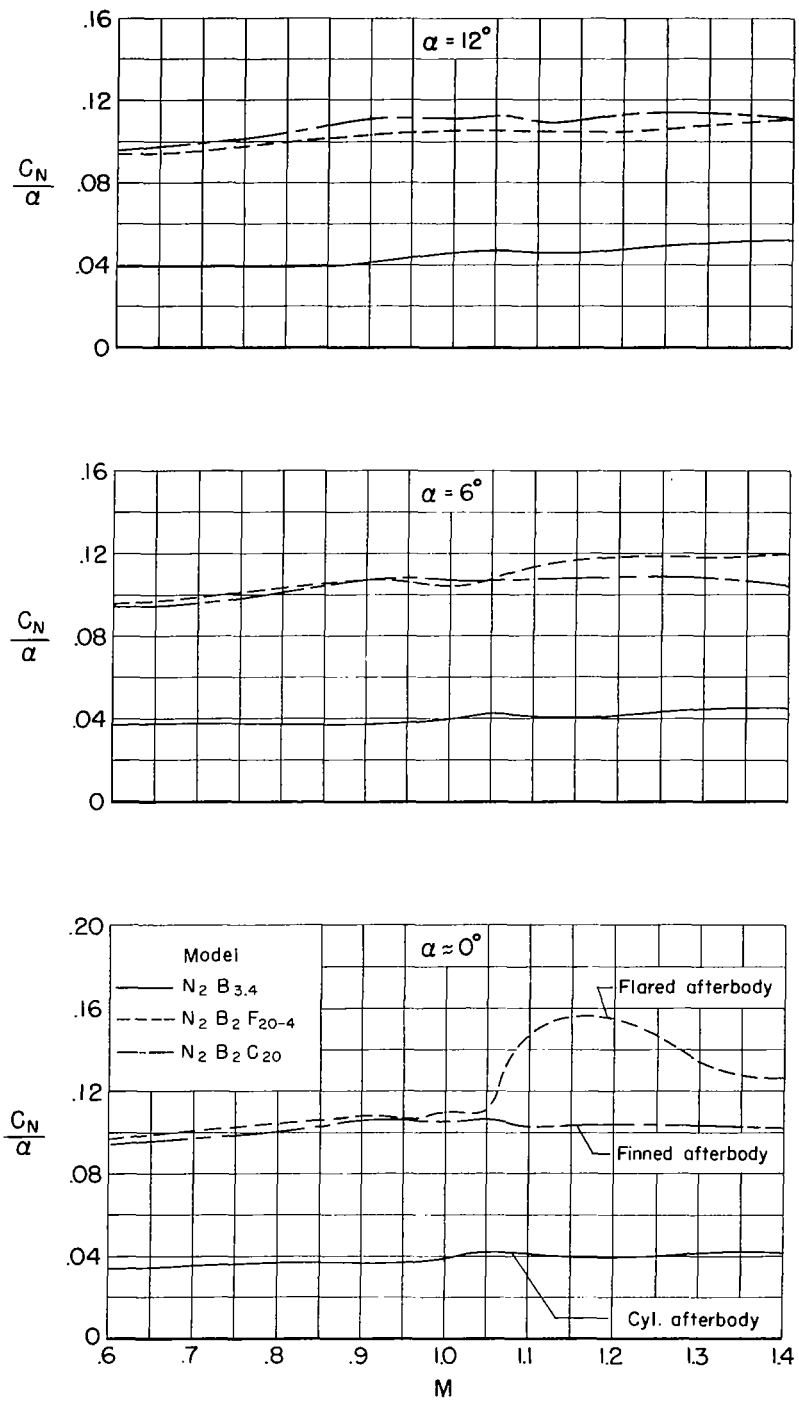

(a) 20° fins and flare

Figure 19.- Variation with Mach number of normal-force parameter.

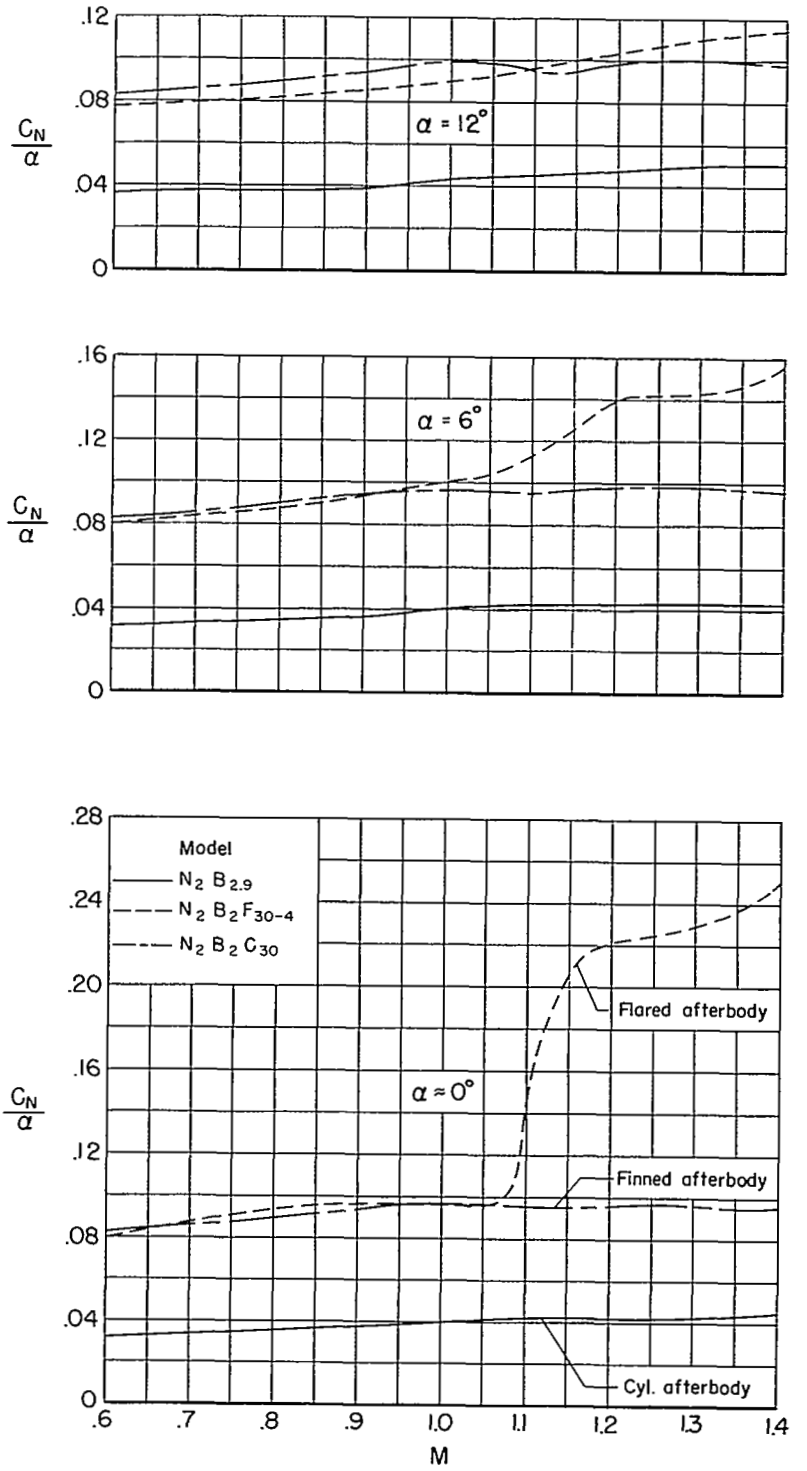

(b) 30° fins and flare

Figure 19.- Concluded.

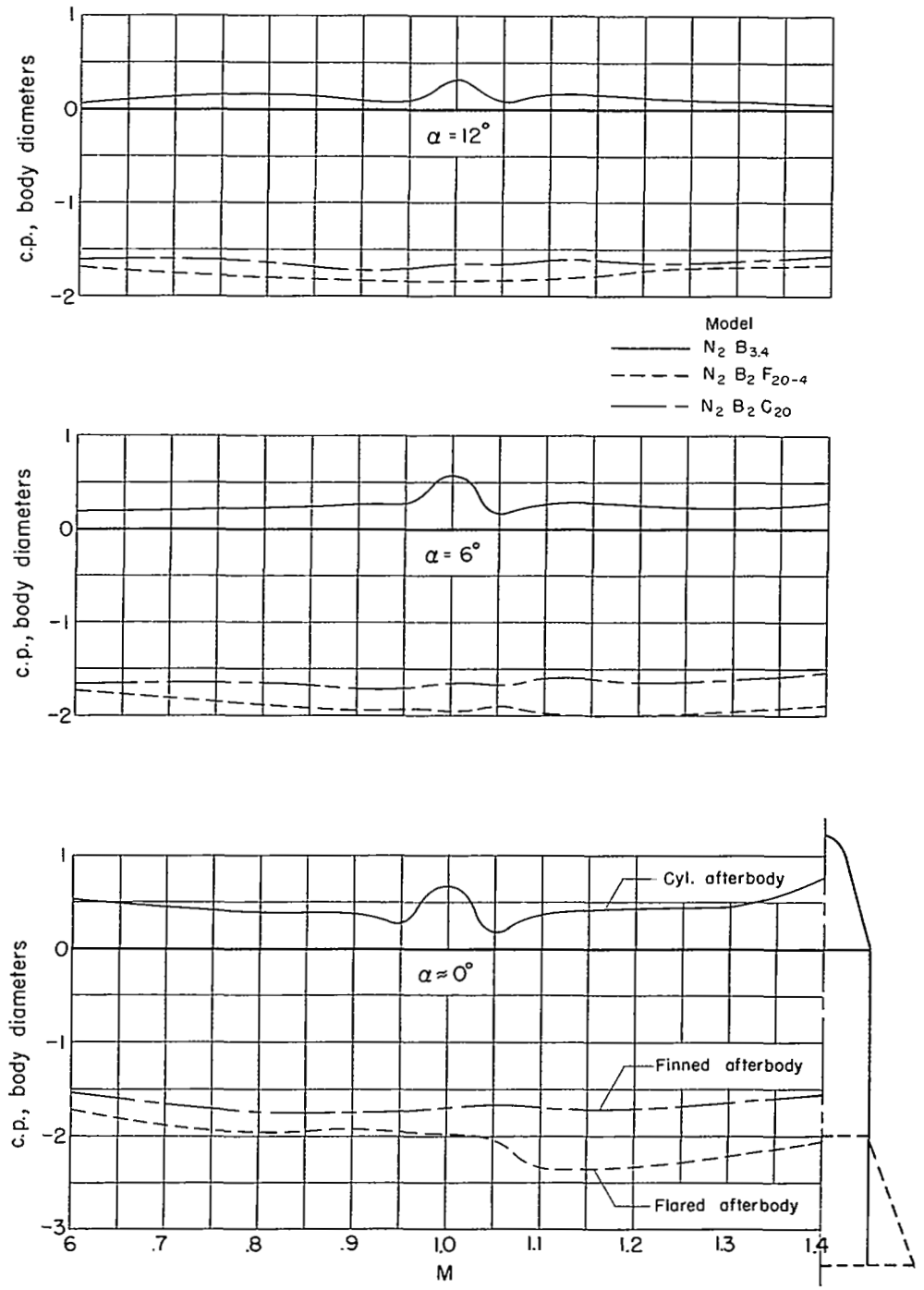

(a) 20° fins and flare

Figure 20.- Variation with Mach number of center-of-pressure position.

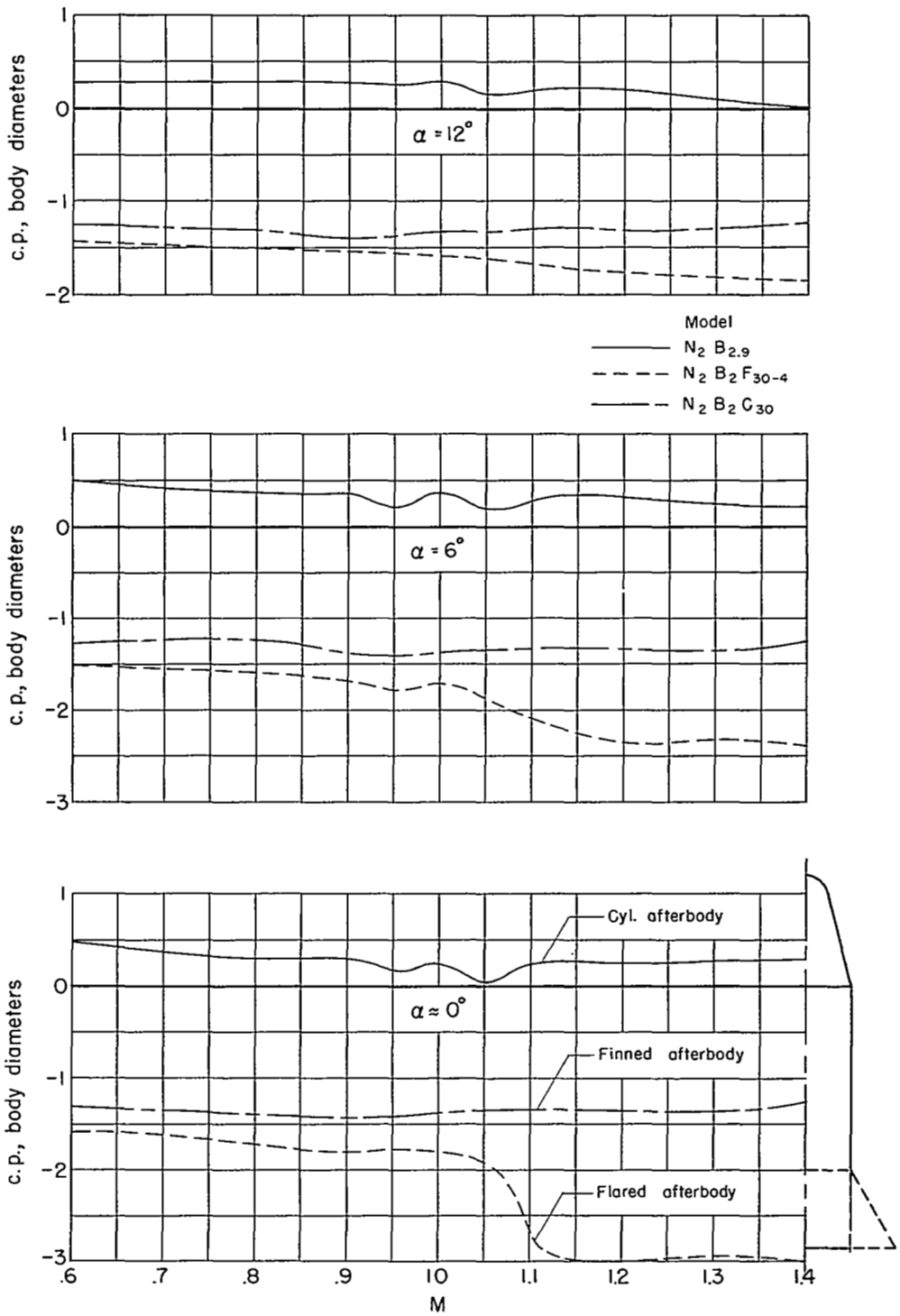

(b) 30° fins and flare

Figure 20.- Concluded.

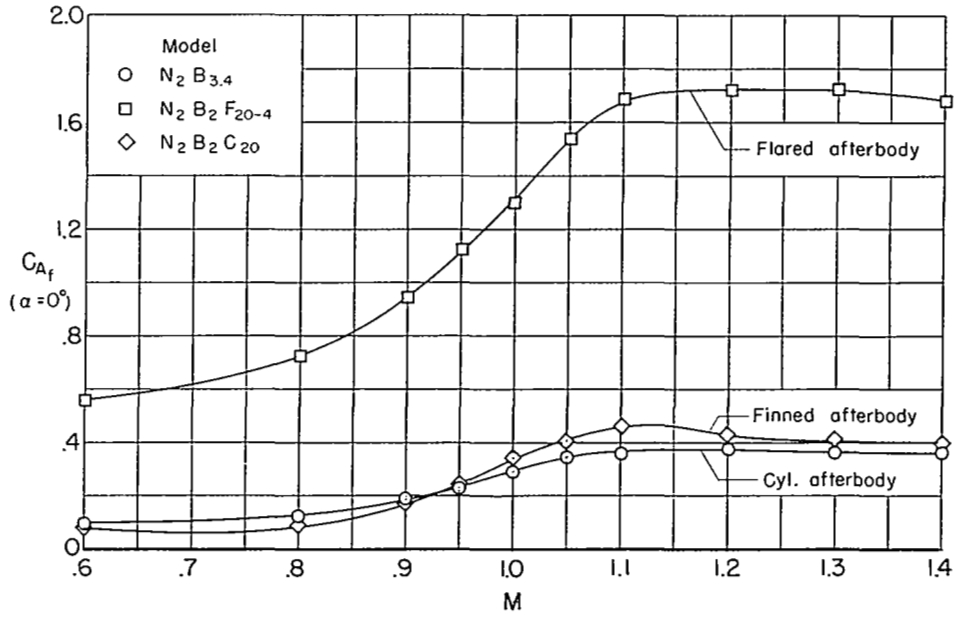

(a) 20° fins and flare

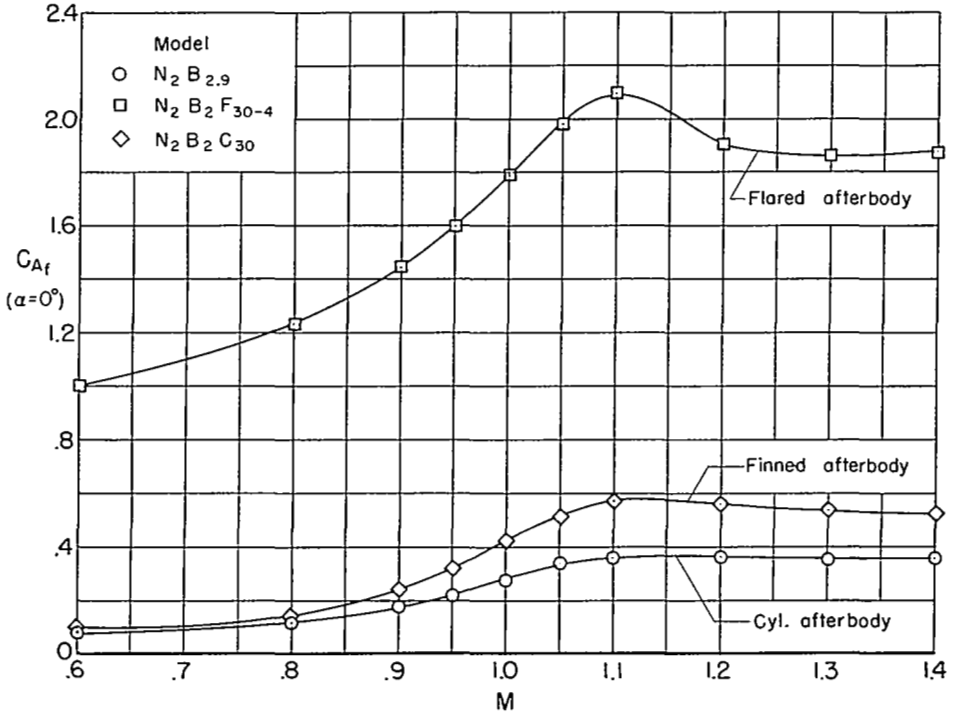

(b) 30° fins and flare

Figure 21.- Variation with Mach number of forebody axial-force coefficient at zero angle of attack.

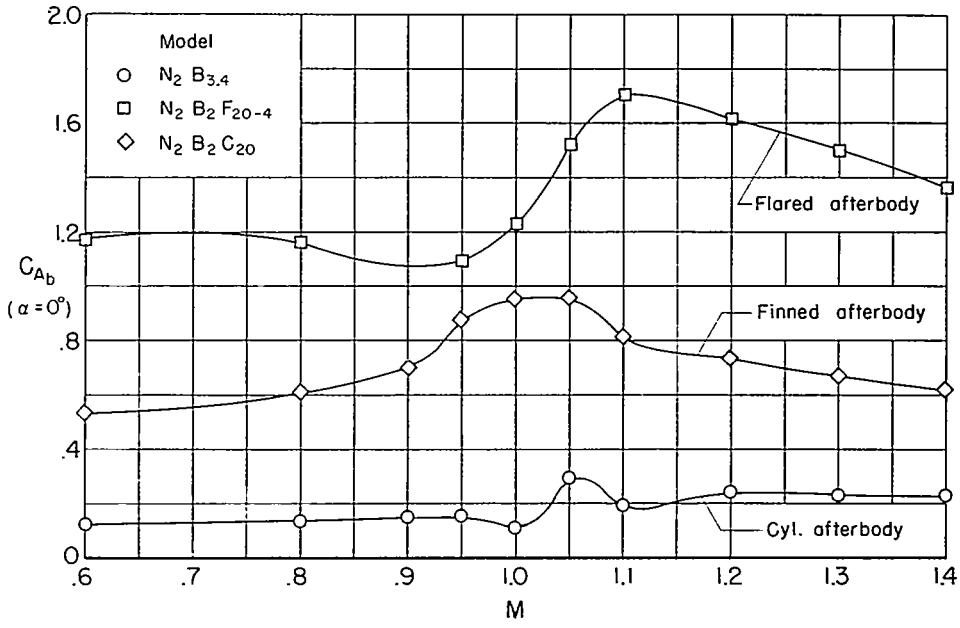

(a) 20° fins and flare

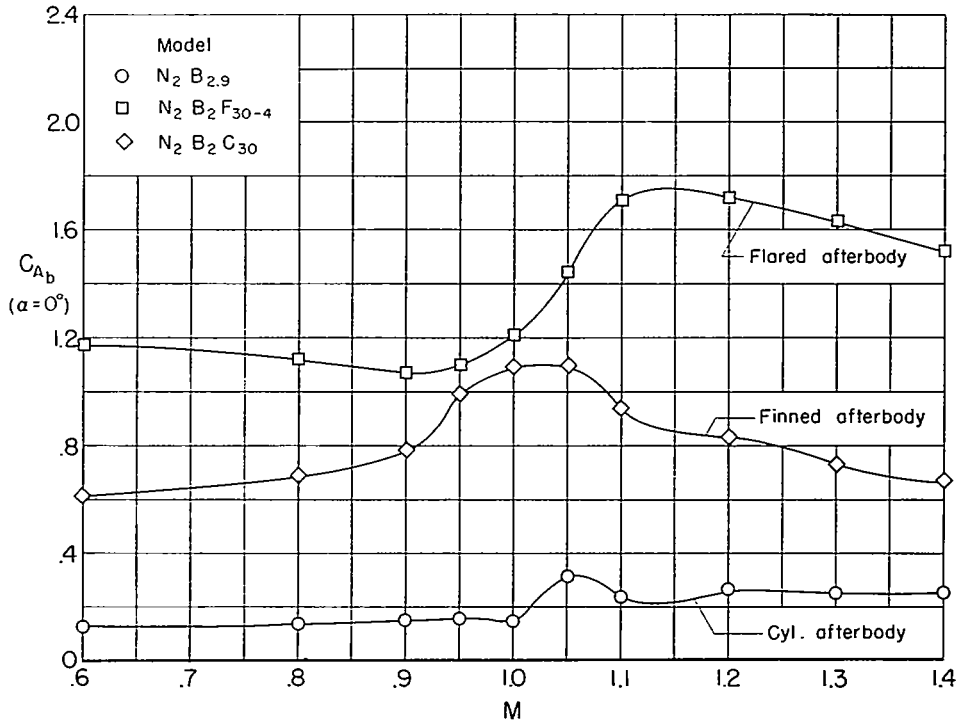

(b) 30° fins and flare

Figure 22.- Variation with Mach number of base axial-force coefficient at zero angle of attack.

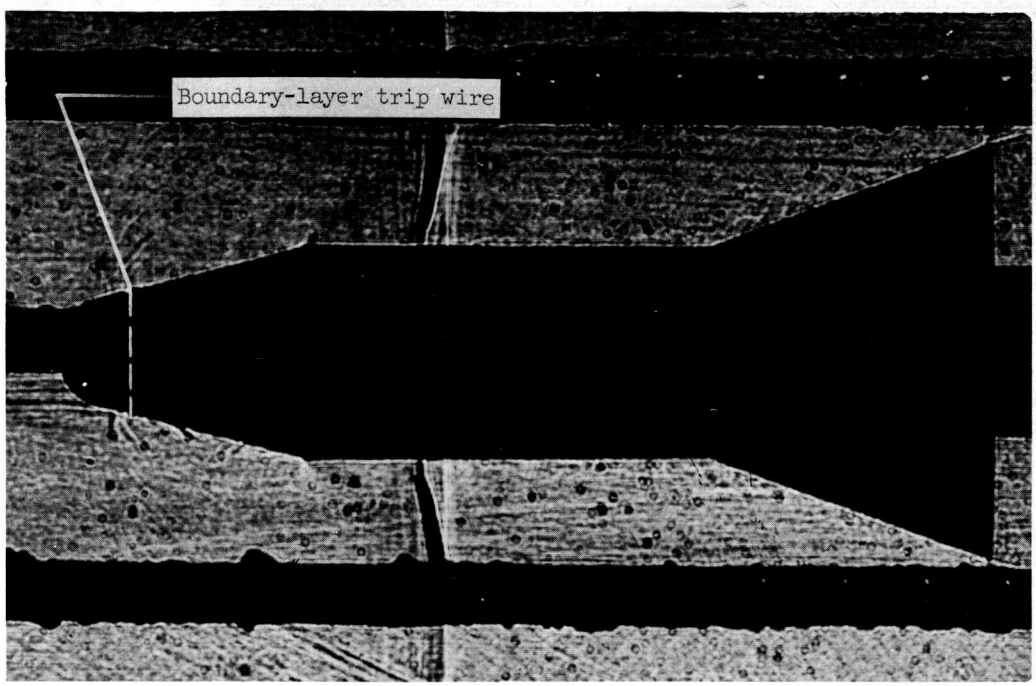

M = 1.0, C_N/α = 0.111

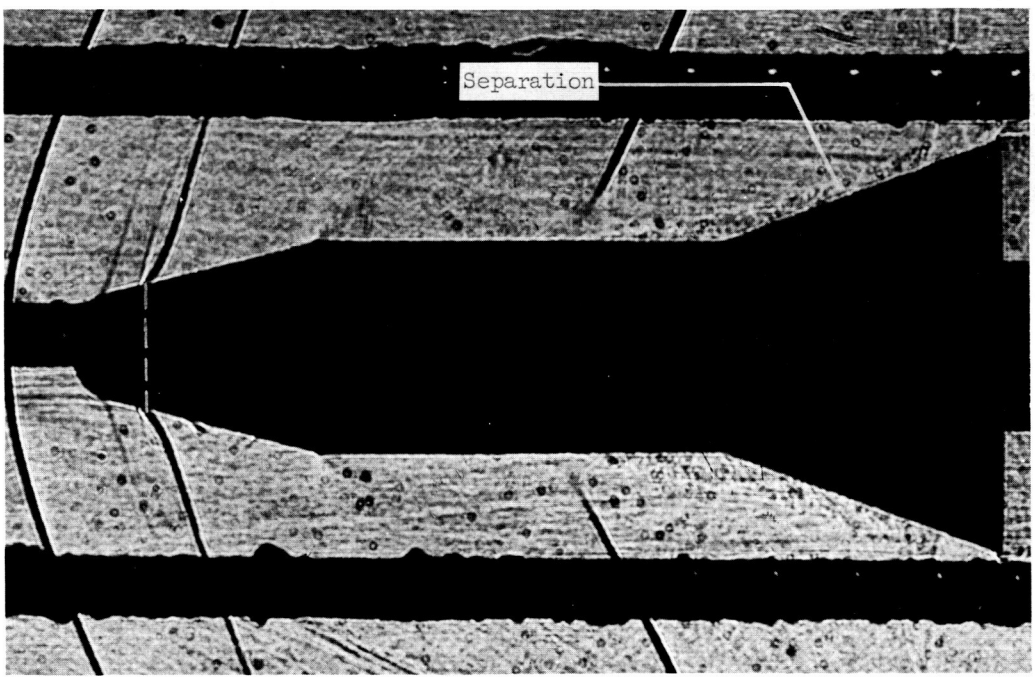

M = 1.2, C_N/α = 0.155

(a) $N_2B_2F_{20-4}$

Figure 23.- Shadowgraphs showing flow patterns before and after onset of separation.

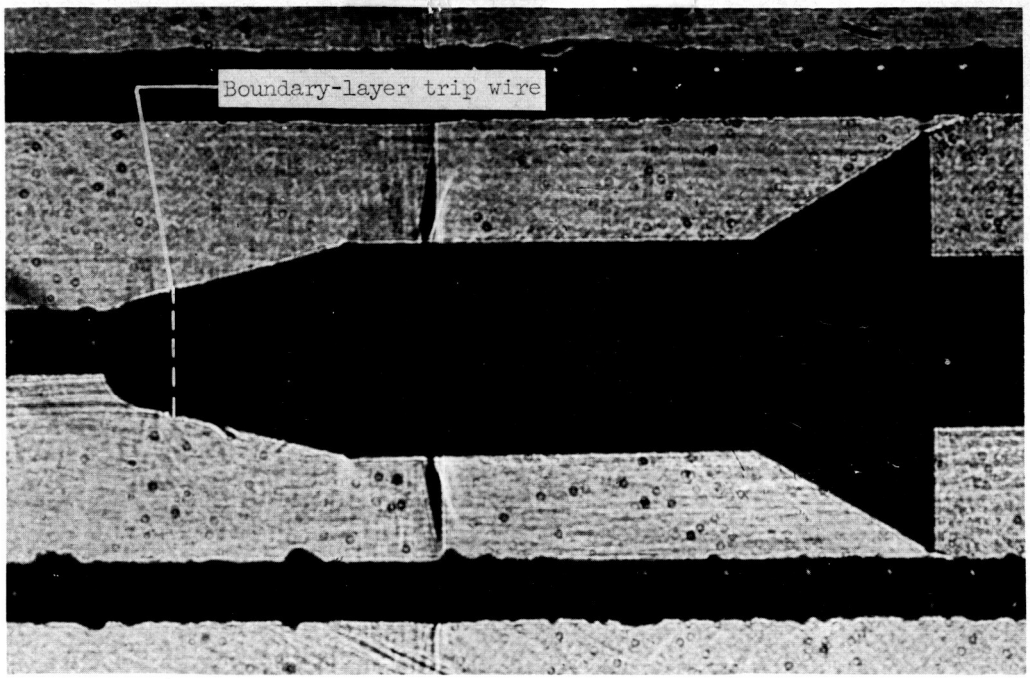

M = 1.0, C_N/α = 0.096

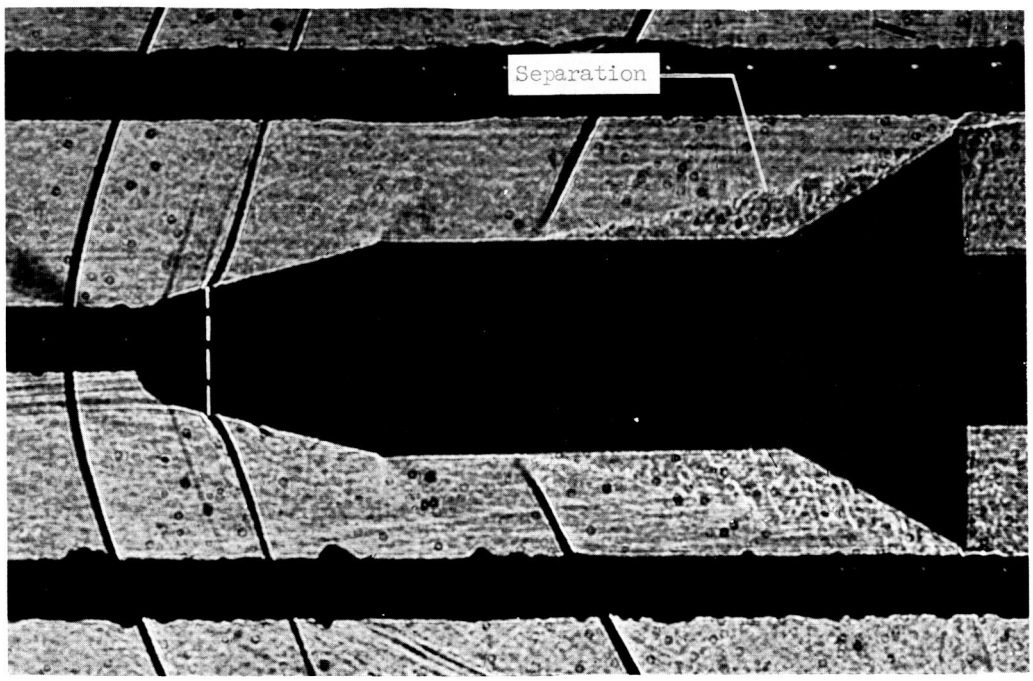

M = 1.2, C_N/α = 0.221

(b) $N_2B_2F_{30-4}$

Figure 23.- Concluded.

NASA - Langley Field, Va. A-260